Simultaneous Reconstruction of Respiratory and Cardiac Motion from Cine Magnetic Resonance Imaging

Kenneth John Batstone

Master's thesis
2014:E28

Lund University

Centre for Mathematical Sciences
Numerical Analysis

CENTRUM SCIENTIARUM MATHEMATICARUM

Abstract

Cardiovascular diseases are currently the leading cause of death in the world, which killed nearly 17 million people in 2011 [3]. For this reason, research in Cardiovascular diseases are of the up-most importance. In this thesis, real-time Cardiac Magnetic Resonance Imaging data is used to create simulated cardiac cycles for multiple phases of the respiratory cycle. By exploring image classification of both cardiac and respiratory cycles with a combination of cycle detection methods (Fast Fourier Transforms, Watershed Segmentation, K-means and locating maximas and minimas) and using a RANSAC method for robustness, interpolated volumes for each respiratory cycle can be created. The use of different interpolation methods are also explored to discover how to produce the best results. In conclusion a Monotonic Piecewise Cubic Spline Interpolation in combination with the use of an optimisation method, to select the most suitable images, proved to be the most accurate method to produce simulated cardiac cycles. The ejection fraction obtained at expiration, from the simulated cardiac cycle, has a value of $55.6962 \pm 1.6199\%$ which is within the current standard normal range of $55 - 70\%$, [14], determined at the same respiratory phase.

As a result of this research, a physiologist will have a useful tool to further understand deformations of the heart due to respiratory motion with relation to the ejection fraction. Further to this, this method could have the potential of being an option for patients in the future. To obtain cardiac MRI data in a faster and less distressing way, the patient would not be required to hold their breath, which can be difficult for some patients.

Acknowledgements

Firstly I would like to thank my supervisors, Einar Heiberg and Sebastian Bidhult, for their support during this thesis and their interesting discussions on the subject. Secondly I would like to thank Gustaf Söderlind for his input on discussing interpolation methods and Per Arvidsson for acquiring the MRI data for me. I would also like to thank the rest of the Lund Cardiac MR Group for their enthusiasm in research, creating an inspirational environment.

On a more personal note, I would like to thank my parents, Paul and Elizabeth Batstone, my partner's parents, Stanley and Monica Dorozynski and my partner Karolina Dorozynska, whom all supported me through my academic studies.

Contents

1 Introduction

Cardiovascular diseases are currently the leading cause of death in the world, which killed nearly 17 million people in 2011 [3]. For this reason, research in Cardiovascular diseases are of the up-most importance, particularly for the Western World. Due to the continuing development of computing and medical imaging, new ways of approaching Cardiac research are emerging. Through the use of Magnetic Resonance Imaging (M.R.I.), the heart can be assessed in a non-invasive way.

The Lund University Cardiac MR Group use MRI technology to develop a better understanding of how the heart functions to a much greater extent. By using MRI techniques new aspects of pumping physiology of the heart in vivo can be seen and in doing so be able to assist clinical physiologists in their understanding of the heart.

In recent developments, techniques have emerged so an MRI machine can acquire real-time data. Thus, detailed studies of motion can be observed. This is of significant importance because now possible to begin to understand how small changes within the body affect the physiology.

The current method to obtain data requires the patient to hold their breath while the MRI machine takes images at specified stages of the cardiac cycle when criterion are met using an Electrocardiogram. This is called a gating method. In research published in 2008, [4], a method was developed where the patient was free to breathe during the scan and images were taken during all cardiac cycle phases. Here real-time acquisition was combined with a post processed gating method in order to correct for respiratory motion and enhance the real-time image quality. This research provided the inspiration for this thesis work.

2 Aim

In this thesis, real-time Cardiac Magnetic Resonance Imaging data is used to create simulated cardiac cycles for multiple phases of the respiratory cycle. This makes it possible to observe how the respiratory motion deforms the heart, which is of interest for physiologists. To achieve the main aim of the thesis a method is developed which encompasses the following four key stages:

1. Creating a classification method to accurately determine the respiratory motion of the heart in real-time Cardiac Magnetic Resonance Imaging data.
2. Creating a classification method to accurately determine the Cardiac cycle of the heart in real-time Cardiac Magnetic Resonance Imaging data.
3. Creating a method to construct interpolated cardiac cycles for each of the respiratory classes.
4. Analyse the interpolate cardiac cycles to determine differences in left ventricle volumes due to respiratory motion.

In addition these aims, by creating a method as described, it could have the potential of being an option for patients in the future, to obtain cardiac MRI data in a faster and less distressing way as the patient would not be required to hold their breath, which is also difficult for some patients.

3 Background

3.1 Physiological Background

3.1.1 Human Heart

The heart is divided into four connected chambers by heart valves. The two lower chambers are called the left and right ventricles which are separated by a septum. The purpose of the right ventricle is to pump deoxygenated blood to the lungs to be oxygenated and the left ventricle receives oxygenated blood, via the left atrium, and pumps it to the aorta and around the body. Since the left ventricle pumps blood to the rest of the body it has thicker myocardium (cardiac muscle) walls.

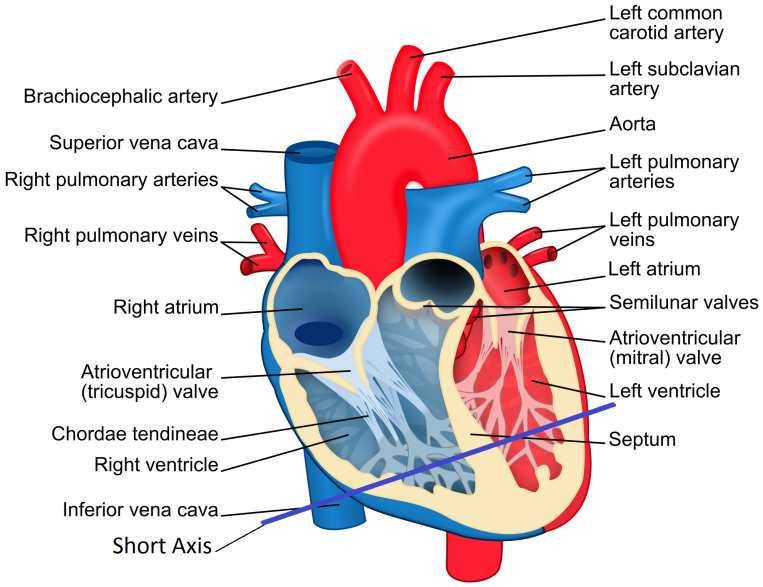

Figure 1: Diagram of the Heart [6]

3.1.2 Magnetic Resonance Imaging (MRI) Physics

MRI is an imaging technique that uses strong magnetic fields and radio waves to image a patient. It is particularly effective due to the large percentage ($\sim 60\%$) of water that makes up the human body. The hydrogen in the water has magnetic moments which can be influenced by a powerful magnetic field outwith the body. When a magnetic field is induced the moments of the protons in the hydrogen align with the magnetic field.

An electromagnetic field in the radio range is then turned on which alters the protons relative alignment. When the radio waves are then turned off the protons are realigned with the magnetic field causing a change in magnetic flux. As a result this changes the induced voltage in the receiver coils and produces a measurable signal.

A modern MRI machine operates around 1.5-3 Tesla and the magnetic field is produced using a superconducting alloy niobium-titanium cooled to 4K with liquid helium. The frequency at which the proton resonates depends on the strength of the magnetic field around the proton. By applying magnetic fields that vary linearly over orthogonal locations, selected slices can be imaged. The image is obtained by taking a 2-D Inverse Fourier transformation of the corre-

sponding resonance frequencies of the protons and calculate a corresponding spatially resolved image.

The T1 relaxation time is a measure of how quickly a group of protons moments, $\mathbf{M} = (M_x, M_y, M_z)$, to return to 63% of the direction of magnetic field, M_0 for magnetic field $\mathbf{B}$, after the radio pulse, which is also referred to as the spin-lattice relaxation time. This time differs in certain materials and with this knowledge, different contrast weighting can be produced on the image to emphasize selected tissues.

The T2 relaxation time is a measure of how quickly a group of protons moments to return to 63% of the direction perpendicular to that of magnetic field after the radio pulse, which is also referred to as the spin-spin relaxation time. This time also differs in certain tissues.

These relaxation times are then used to describe the change in magnetic moments which is characterised by the Bloch Equation.

$$\frac{d\mathbf{M}}{dt} = \gamma \mathbf{M} \times \mathbf{B} - \frac{M_x}{T2}\hat{\mathbf{x}} - \frac{M_y}{T2}\hat{\mathbf{y}} - \frac{M_z - M_0}{T1}\hat{\mathbf{z}} \tag{1}$$

Where the gyromagnetic ratio for Hydrogen is $\gamma = 2.68 \times 10^8$ rad/s/T.

To produce an image, first the demodulated magnetic resonance signals, $S(t)$, generated by the precessing molecules in magnetic field gradient $\mathbf{G}$ are measured. This equates to the Fourier transform of the spin density, ρ, which is given by the equation;

$$S(t) = \rho(\int_0^t \mathbf{G}(t)dt) = \int \rho(\mathbf{r}) e^{2\pi i (\int_0^t \mathbf{G}(t)dt).\mathbf{r}} d\mathbf{r} \tag{2}$$

This in turn can produce an image,I, by using a inverse Fourier transform and making the substitution $\mathbf{k}(t) = \int_0^t \mathbf{G}(t)dt$ the image is represented by, [15];

$$I(\mathbf{r}) = \int S(\mathbf{k}(t)) e^{-2\pi i \mathbf{k}(t).\mathbf{r}} d\mathbf{k} \tag{3}$$

3.1.3 Segment

Segment is a commercial version of the software package sold by the company Medviso AB and developed by Lund Cardiac MR Group [5]. This program is used for viewing and processing Cardiac Magnetic Resonance Imaging data. Some of the features includes left and right ventricle segmentation, Strain analysis and flow analysis.

In this thesis, the developed method will work in conjunction with Segment, using some of the existing function and data structures with the view to make a plug-in in a new Graphical User Interface.

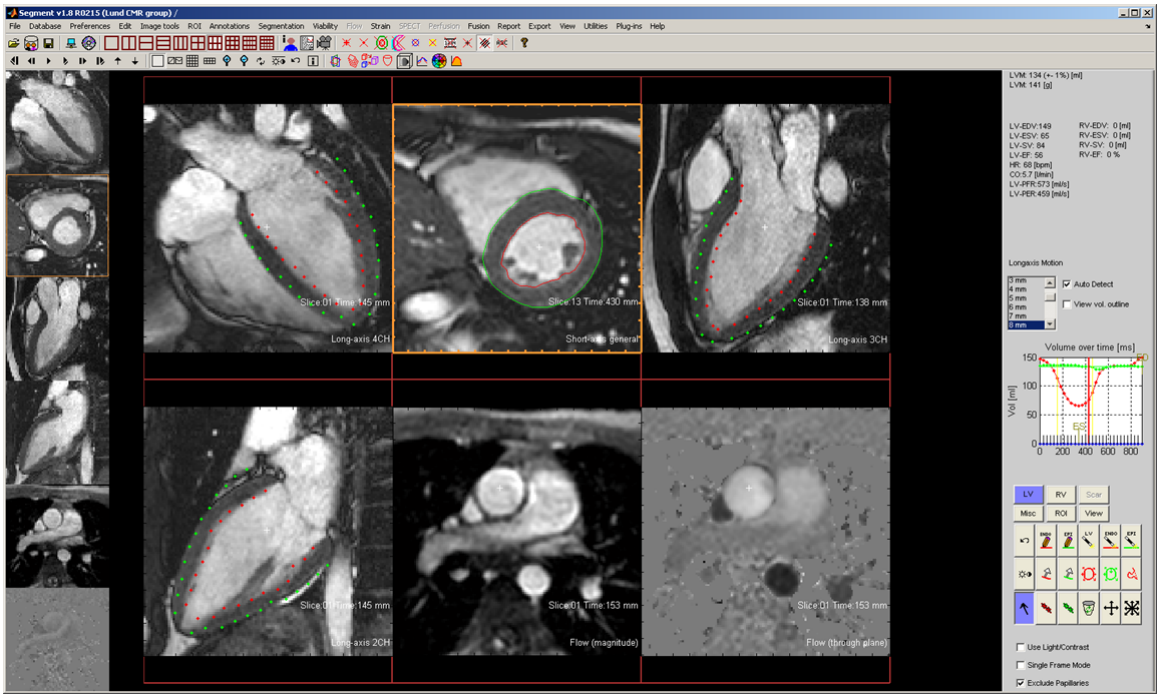

Figure 2: Screen shot of Segment [5]

3.2 Mathematical Background

3.2.1 Morphology

Erosion is a process that can be performed on a binary image with regions of foregrounds and background. Using a small shape, $B \subset \mathbb{Z}^2$, which in most cases a circle, the origin of that shape is then scribed around the edges between foreground, $A \notin \emptyset$, and background, $C \in \emptyset$. Any of the foreground region that falls beneath the small shape becomes background.

$$A \oplus B = \{x|((\hat{B})_x \cap A) \subseteq A\} \tag{4}$$

Dilation is the opposite of erosion. The small shape follows the edge and any of the background region that falls beneath the small shape becomes foreground.

$$A \ominus B = \{x|(\hat{B})_x \cap A\} \tag{5}$$

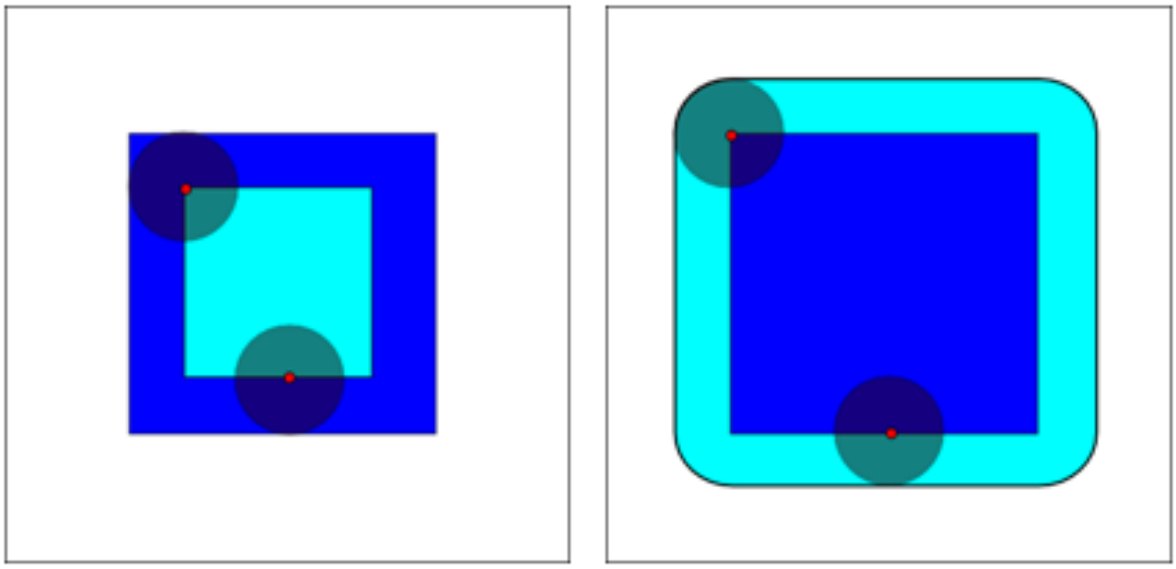

Figure 3: Examples of erosion (left) and dilation (right)

3.2.2 Histogram Equalization

The histogram method is used to increase the global contrast of an image. This is done by redistributing the intensities of every pixel so the cumulative histogram is linearly monotonic.

For some $N \times N$ image with a histogram, $H_0(p)$, with grey-levels $p = \langle p_0, p_k \rangle$, we find a transform $q = T(p)$ so that our new histogram equalized image has a uniform distribution of pixel intensities, $q = \langle q_0, q_k \rangle$ with a histogram $H_1(q)$.

Due to the monotonicity of the transformation, it implies that:

$$\int_{q_0}^{q} H_1(q)\, dq = \int_{p_0}^{p} H_0(p)\, dp \tag{6}$$

and that H_1 has a uniform density such that:

$$H_1(q) = \frac{N^2}{(q_k - q_0)} \tag{7}$$

From this we can see that:

$$\int_{q_0}^{q} \frac{N^2}{(q_k - q_0)}\, dq = \int_{p_0}^{p} H_0(p)\, dp \tag{8}$$

which can be rewritten as:

$$q = T(p) = \frac{(q_k - q_0)}{N^2} \int_{p_0}^{p} H_0(p)\, dp + q_0 \tag{9}$$

and written in the discrete space as:

$$q = T(p) = \frac{(q_k - q_0)}{N^2} \sum_{i=p_0}^{p} H_0(i) + q_0 \tag{10}$$

3.2.3 RANdom SAmple Consensus (RANSAC)

The RANSAC method is an iterative method used to robustly estimate a mathematical model. The idea is that the data consists of noise, which can cause issues with making an accurate model. By choosing a random subset of the data to estimate the model, we can hopefully remove noisy data that skews the model. This method is repeated for a set number of iterations and the best fit, based on a defined cost, usually a measure of how close the model compares to the whole data set, then the best fit is kept as the model.

The advantage of this method is that it is very robust, and can be used to produce estimated models when only 50% of the data fits the model. It's main disadvantage is that there is no end to the number of iterations that should be performed to estimate the model. With each iteration, the probability of estimating the correct model improves. With this in mind, the number of iterations can be estimated before hand to see if the RANSAC method is viable option.

To ensure the total probability, p (usually set to 0.99), of finding the correct model, we estimate, u, to represent the probability of a selected data point that is an inlier. The number of iterations, N, is estimated to be:

$$N = \frac{log(1-p)}{log(1-u^m)} \tag{11}$$

where m is the minimal number of selected data points required to estimate the model [1].

3.2.4 K-means Clustering

K-means Clustering is a method of finding clustered subsets within a set of data points, $(x_1, .., x_n)$. To initialise this method we must first define the number of clusters k we wish to find. By then choosing, k, data points and allocating them as cluster centres, μ_i for $i = 1, ..., k$, we can define for each data point which cluster it belongs to by looking at the nearest cluster centre. The cluster centres are then updated as the mean of the cluster subset, $S = S_1, ..., S_k$ and the data points are then reclassified according to their nearest cluster centre again. This is then repeated until the cluster centres have converged. The K-means clustering problem solves:

$$\arg\min_{S} \sum_{i=1}^{k} \sum_{x_j \in S} \|x_j - \mu_j\|^2 \tag{12}$$

The method can encounter problems finding clusters if the initial centres are too close to each other and can sometimes converge to local minimums but in general the k-means algorithm is run multiple time to avoid these problems and on well clustered data, it is robust [2].

3.2.5 Monotonic Piecewise Cubic Spline Interpolation

The Monotonic Piecewise Cubic Spline interpolation is a form of Cubic Hermite spline interpolation that acts to preserve the monotonicity of the spline. By preserving the monotonicity, the interpolated spline has no overshooting between two data points in order for the spline to fit the knots.

Let there exist a set of data points, $x_1 < x_2 < ... < x_n$, that partition the interval $I = [x_1, x_n]$. The aim is to create a piecewise cubic function

$$p(x) = f_i,\ i = 1, 2, ..., n \text{ for } p(x) \in \mathscr{C}^1[I] \text{ and is monotonic} \tag{13}$$

where f_i is the value of the point x_i. Between the data points the cubic polynomial s represented by

$$p(x) = f_i H_1(x) + f_{i+1} H_2(x) + d_i H_3(x) + f_{i+1} H_4(x) \tag{14}$$

where the gradient of each data point is $d_i = p'(x_i)$ and the Hermite basis functions are $H_k(x)$ for $k = 1, 2, 3, 4$. As it can been seen in Equation (14), in order to maintain monotonicity, d_i must be calculated in such a way to stop overshooting.

In the Fritsch - Carlson method, [13], a 5-part algorithm was proposed for calculating monotonic splines.

1. Calculate the gradient for each of data points, $\delta_i = \dfrac{f_{i+1} - f_i}{x_{i+1} - x_i}$ for $i = 1, ..., n-1$
2. Initialise the gradients between the data points, $d_i = \dfrac{\delta_{i-1} + \delta_i}{2}$ for $i = 2, ..., n-1$
3. For $i = 1, ..., n-1$, if $\delta_i = 0$ then $d_i = d_{i+1} = 0$ and these points are ignored for the next 2 steps since the spline must be flat.
4. Two gradient ratios are calculated to test for monotonicity, $\alpha_i = \dfrac{d_i}{\delta_i},\ \beta_{i-1} = \dfrac{d_i}{\delta_{i-1}}$, if any of these are less then zero then for those points $d_i = 0$
5. Finally to maintain monotonicity, the restrain $d_i = \dfrac{3\alpha_i\delta_i}{\sqrt{\alpha_i^2 + \beta_i^2}}$ and $d_{i+1} = \dfrac{3\beta_i\delta_i}{\sqrt{\alpha_i^2 + \beta_i^2}}$ are used to update the data points gradients.

From these, the Monotonic Piecewise Cubic Hermite splines can be calculated using Equation (14). In Matlab, they use this algorithm called “pchip”, which comes from Fortran code created by D. Kahaner, C. Moler, and S. Nash [12].

3.3 Magnetic Resonance Data

3.3.1 Magnetic Resonance Imaging Machine Specifications

Real-time imaging was performed on 1.5T MR2 Philips Medical Systems Intera at Lund universitetssjukhus,Sweden, using real time bSSFP imaging. The temporal discretization was 218.4 ms for a 250 by 250 by 200 matrix using the software version 1.9 R3420. In real life terms this creates an image of 312.5 mm by 312.5 mm for 43466 ms. The thickness of each image slice is 8 mm. The scanning was performed on a healthy individual using a dual coil.

3.3.2 Magnetic Resonance Imaging Data

From the scan, images for each of the 200 time steps were produce for each slice. Multiple slices at a discretized space are made to span the whole heart so a full 3D volume can be created and each 3D pixel is called a voxel. For processing the image volumes were reduced in size to matrices of 120 by 120 by 200 in the region of interest. This is achieved graphically using segment.

In this thesis, we will only be looking at short axis images of the heart. The short axis is an image plane that cuts through both the left and right ventricle as seen in the Figure 1. An example slice is given in Figure 4.

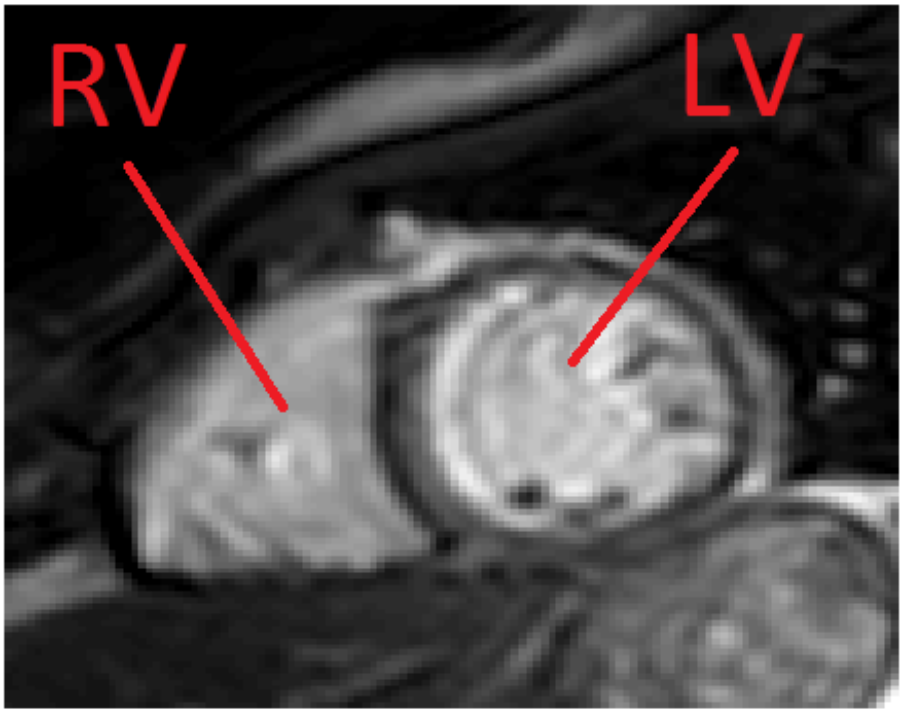

Figure 4: Example of a Cardiac Magnetic image

By imaging multiple adjacent slices over a period of time, 4D data can be acquired, 3D in the spacial domain and 1D in the time domain. A sequence of 1 slice over 6 time frames is

shown in Figure 5, which is an example of the type of data that will be used in this thesis.

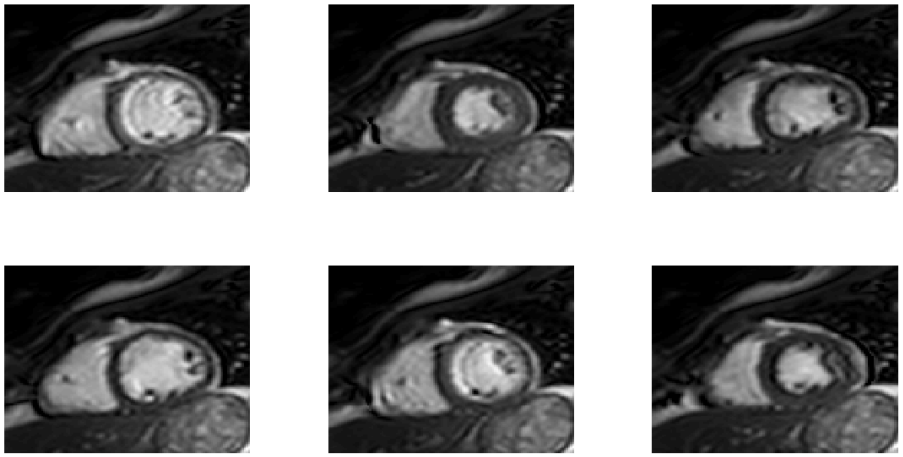

Figure 5: Example of Real-time Cardiac Magnetic sequence

4 Method

4.1 Find the Positions of LV and RV

To start the method of reconstructing the cardiac motion at different phases of the respiratory cycle, we must first be able to measure the respiratory motion. To do this the bottom of the right ventricle, which is not strongly affected by the motion of the heart beating, was monitored as there is a clear contrast between the right ventricle and the heart walls. A simple way would be to create an image plane that cuts through the time domain by resampling along the line by nearest neighbour interpolation for each of the time frames. This is called "mmode" in segment. Below is an example of the mmode, Figure 6.

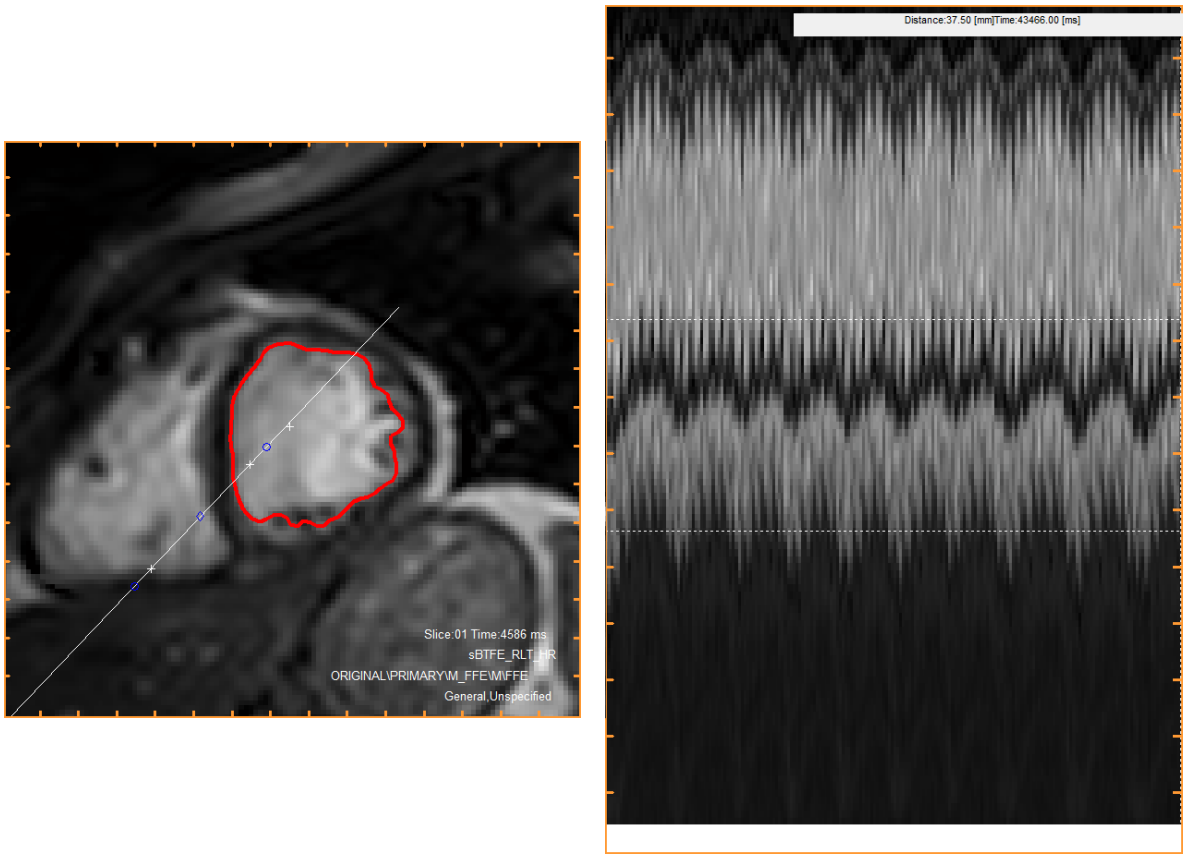

Figure 6: Examples of MRI image with left ventricle segmentation in red and the mmode line in white (left) and mmode image (right)

The best place for the mmode line be would be cutting through the left ventricle and the bottom of the right ventricle. For this, an automatic process was created with the option for making the adjustment manually. The automatic process first locates the left ventricle, this is achieved by normalizing all the images in the sequence and applying a Gaussian circle to emphasize the centre pixels. Then all the images were multiplied together, over time central pixels of the left ventricle are unaffected by both cardiac motion and respiratory motion meaning that when multiplied together this central point becomes the maximal area in the produced image. By using this point, the left ventricle is located and Segment's segmentation algorithm for the left ventricle can be used to find the perimeter of the left ventricle for all time steps.

The next process is to locate the right ventricle. By converting the sequence of images to black and white images, through image thresholding, the two largest objects are both the ventricles. Since the location of the left ventricle already known, this can be removed from the black and white images, thus leaving the right ventricle and noise. The noise was cleared by using a morphology process called opening, which is erosion followed by dilation. Then for each image in the sequence the bottom of the right ventricle is located since the right ventricle is triangular, then the mmode line is calculated to best fit the bottom of the right ventricle and the centre of the left ventricle.

4.2 Detection of Respiratory Motion

The mmode image is separated into two high intensity regions, which are the left and right ventricles, as seen in Figure 6. Again this image is transformed into a black and white image by thresholding. Then using the left ventricle perimeter data, the left ventricle region was removed and the bottom of the right ventricle was measured by creating a data point for each time step by locating the edge between the right ventricle and the heart wall furthest away from the left ventricle. These points were then smoothed to create a smooth line which can accurately measure the respiratory motion. This process was iterated for 11 steps by moving the mmode line in a perpendicular direction, 5 steps in each direction. At each line location rotations were made from the centre of the line through 15 degrees in each direction. This creates a large data set in which the respiratory motion can be seen and reduces errors within our data.

4.3 Fitting a Plane to Respiratory Motion surface

With this large data set of around 66000 data points for a sequence of 200 time frames, a LOESS (locally weighted scatter-plot smoothing) plane was used to remove outliers and errors were the detection of the respiratory motion was incorrect. Then a biharmonic plane was fitted to the data using Matlabs built in function. This accurately fits plane that are 2 dimensionally harmonic, which is ideal for this problem as the respiratory motion is harmonic, as seen in Figure 7. After the fitting was complete, the data was then normalize for each of the respiratory motion iterations, in Figure 7, so the data is corrected for shifts when different angles of mmode were used, for example. From this normalised data, a discretization of 1 along the iterations axis was used to reduce the number of points but also the surface will have the correct data form so it may be represented in an image form.

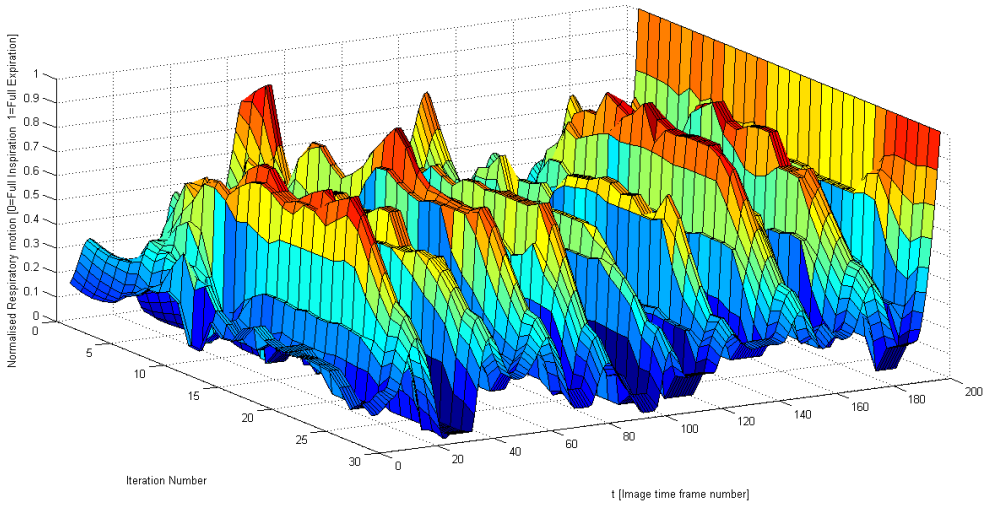

Figure 7: Example of the large respiratory cycle data in normalised surface form

4.4 Finding Respiratory Cycles

Now the data is in a form that can be analysed more easily, the respiratory data can start to be classified. The first part of this classification is to detect the different breathing cycles. Since data characteristics from various patients can be different, such as the temporal resolution, different methods that could detect each of the cycles had there advantages and disadvantages. Since not one method would satisfy data of all temporal resolutions, the decision was made to create multiple methods to analyse the respiratory motion so jointly the machine can come to a logical decision. The methods used are Fast Fourier Transform, Watershed segmentation, K-means and simple peak finding, each will be explained in the following sections. By using these methods the turning points can be determined. The turning points are locations where the data is a local maxima or mininas, the first differential is 0 and the second differential is $\neq 0$.

4.4.1 Fast Fourier Transform

By averaging the points along the number of iteration on Figure 7, a 2-D graph was created showing the average respiratory motion. From this, the 2-D graph was past through a Fast Fourier Transform algorithm to transform the data into the frequency domain, see Figure 8. The maximum magnitude of the frequencies was calculated, the frequency was then converted so it was represented by a period since $period = \dfrac{1}{frequency}$, and the location of the maximum frequency was the period of the respiratory cycle.

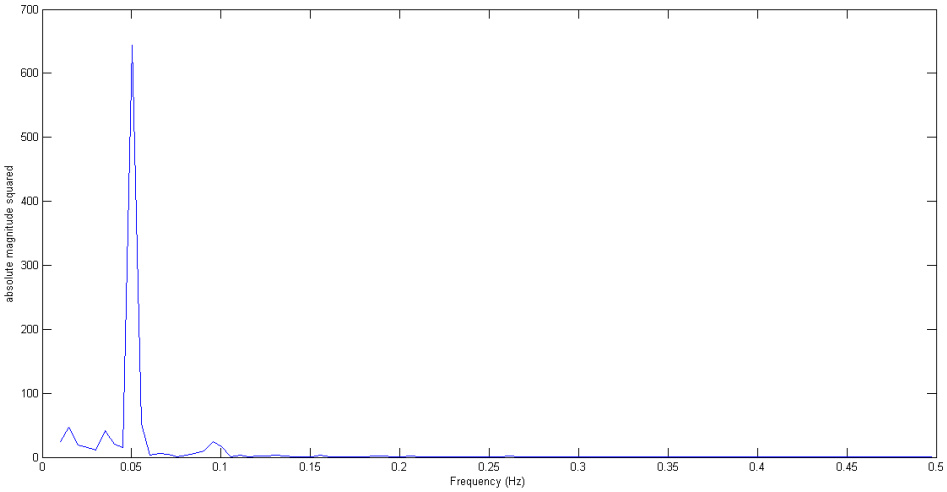

Figure 8: Example of the result from a Fast Fourier Transform to calculate the frequency of the respiratory motion

The turning points of the respiratory motion was also analysed and by using the period as a guide, the starting turning point for the cycles were calculated by viewing which of the turning points in the region $t < (2 \times period)$ would best suit the number of turning points evaluated by $card(\{0\ mod(period)\})$, $\forall(turning\ points) \in t$. Once the starting point for the first cycle is found, using the period the algorithm "leap frogs" one period and finds the closest turning point and so on until all cycles are found.

The disadvantage with this method is that the period isn't accurate on a sequence with a low number of time frames otherwise it is a very reliable method.

4.4.2 Watershed segmentation

Watershed segmentation is a method combining similar regions together in an image. Using the respiratory motion data in an image form, Watershed algorithm calculates the edges of the image similarly to canny edge detection. The closed regions then undergoes morpholocial opening to remove small closed regions. Each of the regions are then given a constant value calculated by the average of the pixel intensities within each region. After a small amount of Gaussian smoothing, the respiratory image is converted to a similar image but with block intensity regions, that can seen in Figure 9.

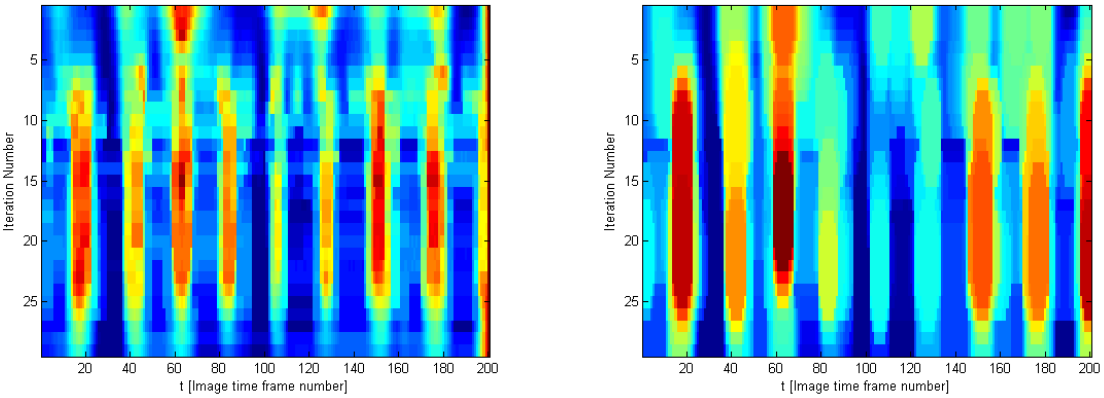

Figure 9: Example of Respiratory Data in Image format(left) and after Watershed segmentation (right).

Like before the new image is then summed along each of the time steps so a 2-D graph is created and the turning points are located. This time a method was used which placed a length of seeds along the each of the turning points times and allowed these seeds to step in the time direction towards the greater intensity until the seeds converged. By allowing the seeds to move and converge, the majority of seed move towards the beginning or end of a respiratory cycle. By repeating this process, eliminating minority locations (i.e. local minimas), this also allows a convergence to the locations of the respiratory cycles, solely. This process can be sensitive to some larger local convergent areas but this method is ideal for sequences with a short period.

4.4.3 K-means

The K-means method of detection is very similar to the Watershed segmentation method but it uses K-means to find the regions of different intensities. In addition to this, K-means regions of 2-D gradients close to 0 were found and K-means regions of minimas for 2-D double differentials, thus regions of potential turning points were found.

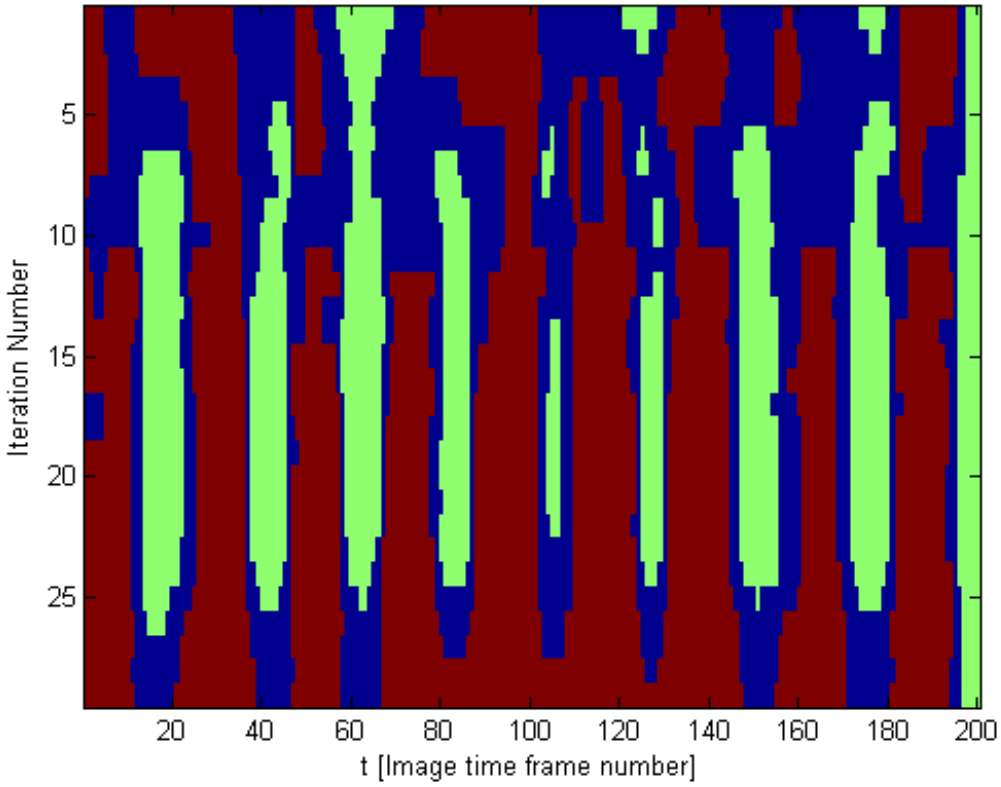

Figure 10: Example of the 3 intensity regions from the respiratory image data when using K-means. This is comparable to Figure 9 and it can be seen that high intensity regions are blue, low intensity red and in between green.

Again this method is ideal for sequences with a short period.

4.4.4 Peak Finding

This is a simple method, which is just summing along each of the time steps and finding turning points, as shown in Figure 11.

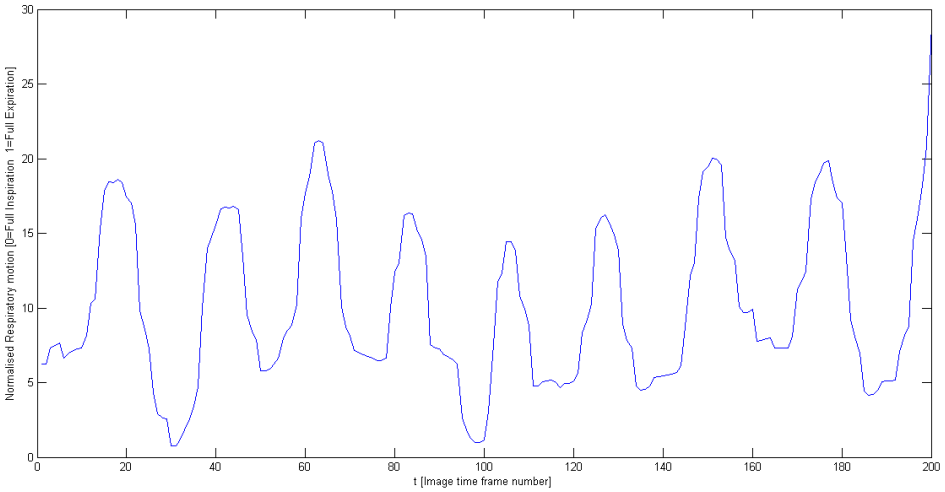

Figure 11: Example of the graph produced when the summation of all iterations are applied.

4.4.5 Logical Decision

Each of the methods output a list of potential locations for the beginning and end of respiratory cycles. Each location is allowed a shift of 3 time steps in each direction and the Fast Fourier Transform method has a doubled weight as it is the more reliable method. If a location has a majority vote, i.e. 3 or more, then that location is a true location, then a new set for true locations is made.

4.5 Classification of Respiratory Cycles

From finding each of the respiratory cycles, these data points are then normalised in both directions, in order to characterise the curve. Looking at the curve in Figure 12, there are two main turning points, at the end of inspiration and at the beginning of expiration.

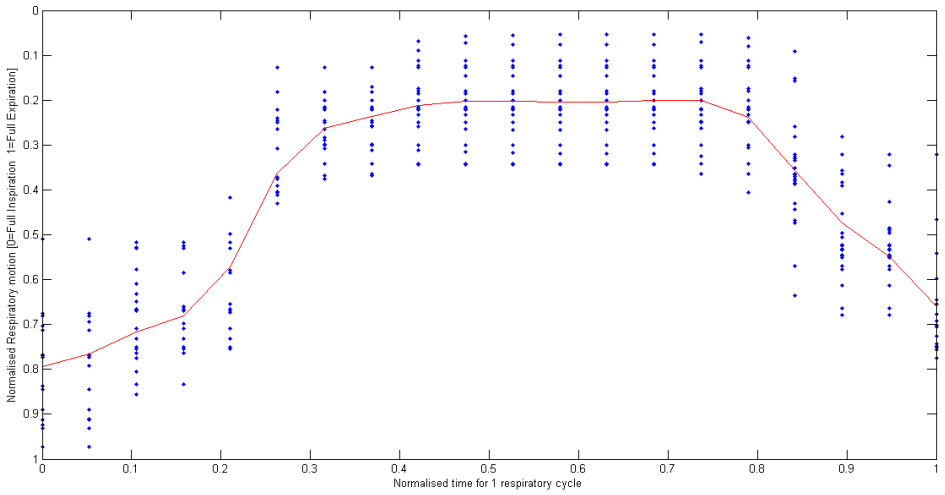

Figure 12: Example of a normalised respiratory cycle data, the points being the raw data from the bottom of the right ventricle and the line is a least squares regression of those points.

To classify this curve, the gradients are use to make an initial classification. All gradients less than or equal to -0.5 are classed as inspiration and all gradients that are equal to or greater than 1 are classed as expiration, everything else are classed as the breath being held. Since the respiratory cycle is a fix cycle, to clear up the initial classification of misclassified points, we use the RANSAC method. To determine the curve, only the locations of the two turning points are required. This in turn reduces the number of iterations to find a suitable fit. Using the formulation in Equation (11), $N \approx 200$ iterations for total probability of 99%. In the costing function for the RANSAC method, two of the points in the region between inspiration and expiration were chosen at random and a fit of the ideal three classes in continuous regions and any matches between the ideal classes and the class from the data was given a point. Extra weight was used for inspiration and expiration within the turning points region to allow for a better fit in these regions. The best fit was chosen to be the highest score and the data can be fitted well, both inspiration and expiration classes were split into a further 3 subclasses based on their respiratory motion positions. These subclasses are derived from 3 equidistant regions from 0 to 1 in the respiratory motion axis.

This leads to a classification as shown in Figure 13. For each of the cycles the numeric values of 1 to 7 are use. Inspiration has classes 1 to 3, full inspiration is class 4 and expiration has classes 5 to 7.

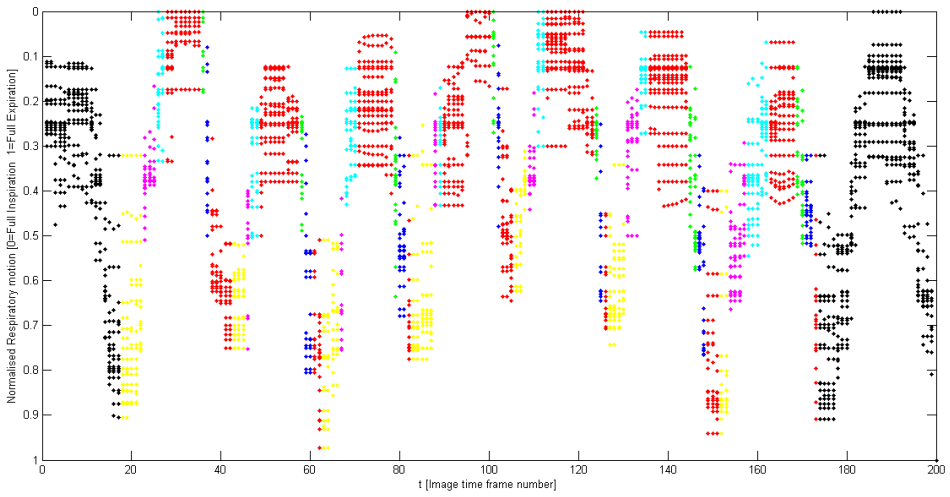

Figure 13: Example of respiratory cycle classified. Each colour represents a specific class.

4.6 Classification of Cardiac Cycles

To classify cardiac cycles, the systole (when the heart contracts) was found by searching for peaks. To do this all the left ventricle perimeters for all time frame, were transformed to cylindrical coordinates relative to a common centre of all left ventricle perimeters. Then by computing the summation of all points for each time frame, the peaks on this left ventricle graph are very clear, as seen in Figure 17. From this, the period was found using a Fast Fourier Transform. To classify the cardiac cycles, the discretization was calculated by $dx = \frac{1}{peak_{i+1} - peak_i}$. Each frame between is allocated a class value of $0 - 0.99$ where the peaks, systole points have the value 0.5. This means that each cardiac cycle has a value which relates to the position in the cardiac cycle on how far the cycle is complete.

4.7 Interpolation of Cardiac Cycles

4.7.1 Initial Method: Smoothing Spline Interpolation

With both the respiratory and cardiac classification, the frame numbers are sorted by there classification so that a list of frame numbers are created for each category. For interpolation, there is a loop for each pixel in the image, when a pixel is chosen, for all the frames in that respiratory cycle, the intensity of the pixel are plotted against their Cardiac inter-beat (RR) interval time. From this, a smoothing spline is fitted to the plot and the interpolated points (which is a discretization of 0 to 0.9 in increments of 0.1) are passed back to fill the interpolated volume. Due to the cyclic behaviour of a cardiac cycle, the first set of frames are copied to the end and vice versa.
A problem with this method is that some of the interpolated images become blurred due to variations in multiple images occupying the same respiratory class and heart beat class. This can be viewed by looking at the left ventricle segmentations in Figure 14.

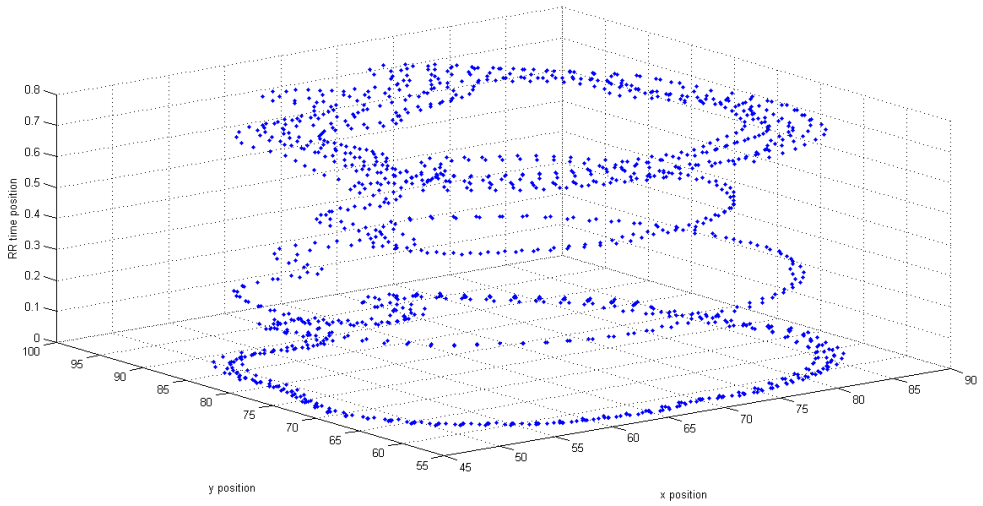

Figure 14: Scatter-plot of all left ventricle plots in one respiratory class.

4.7.2 Alternative Method: Image Selection and Monotonic Piecewise Cubic Spline Interpolation

A solution to this would be a method to choose the best frames when there are multiple frames at one location in RR time. This alternative method will look at all combinations of frames in the whole RR time and create a curved surface to wrap around the contours. This is computed by converting the coordinates to cylindrical coordinates on a regular discretization. From this, the surface with the least radial change, relative to the straight line that best fits the centre of all the contours, will be selected. The only exception to the selection will be around the RR time of 0.5 where we would expect the heart to contract and so the maximal change will be viewed.

The next problem with this is the computational side, by finding all combinations, this can lead to many thousands of combinations of frames. To make it computationally viable, by removing duplicate frames (i.e. when the 2-norm of any 2 left ventricles is very small), then the

number of combinations falls dramatically.

The advantage of this method is that there only exist one frame at any given time step. For this alternative method, a Monotonic Piecewise Cubic Spline Interpolation can be used in the same manner as before but it will pass through all points giving a better image quality.

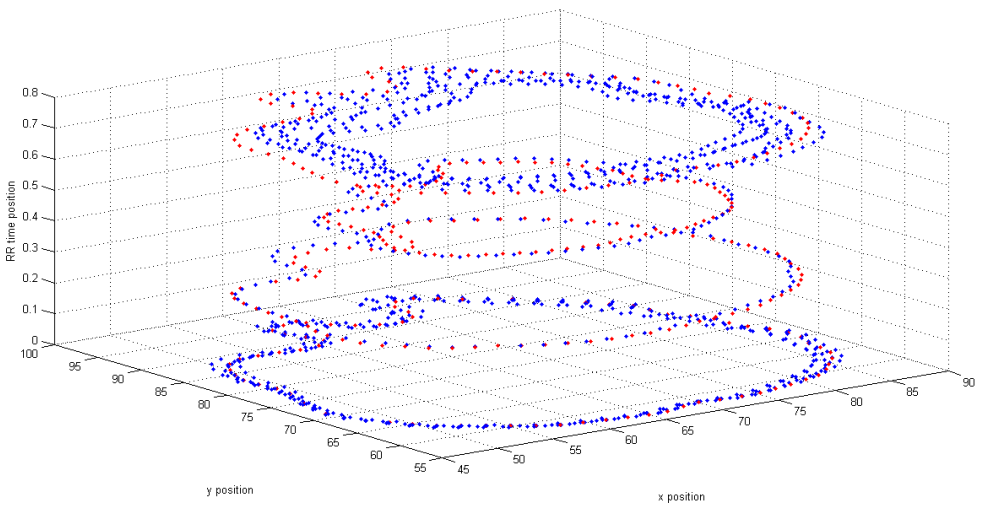

Figure 15: The red points are the left ventricle perimeters that have been selected for the best fit. This is comparable to Figure 14.

5 Results

5.1 Classification of Respiratory Cycles

From the graph in Figure 13 and below in Figure 16, it can been seen that the classification for the respiratory has worked well. Only the two partial respiratory cycles at the edges, which at the black coloured points in Figure 13, have not been classified. This was to be expected since the classification method is gradient based and gradients required multiple points to be calculated so these cannot be determined at the edges.

Looking again at Figure 13, all the other cycles were detected with clear boundaries between cycles.

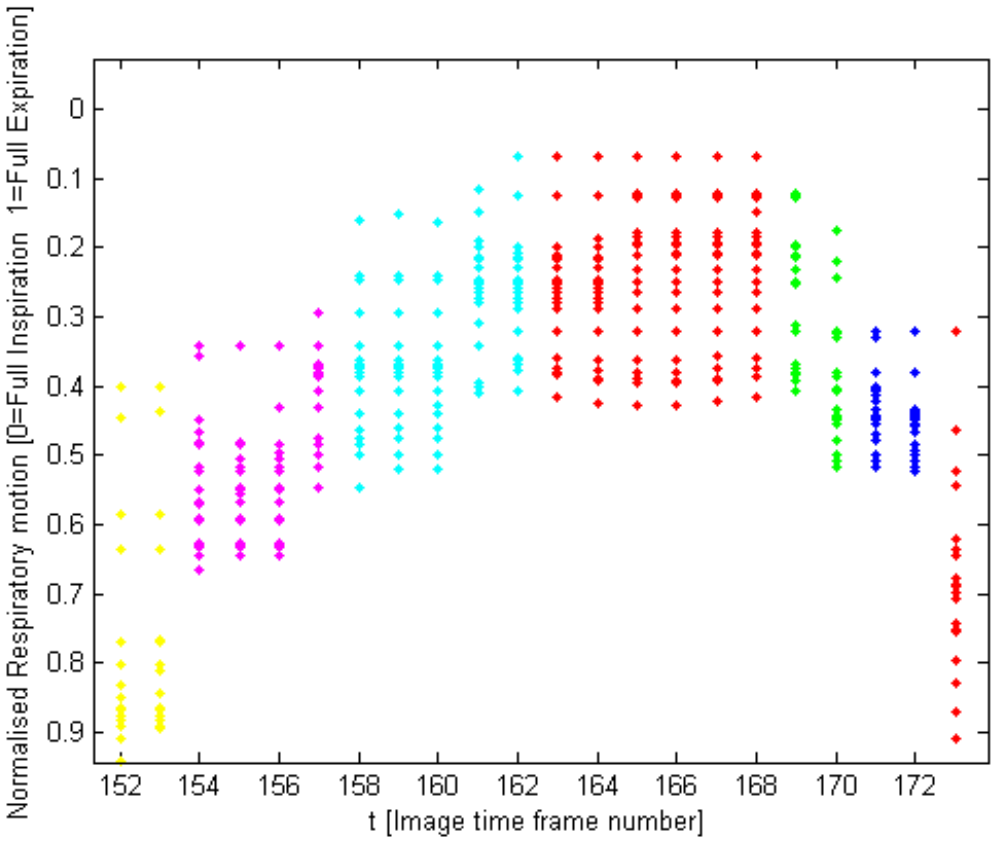

Figure 16: Example of respiratory cycle classified. Each colour represents a specific class.

On closer inspection of Figure 16, class 4, which is in red with a low respiratory motion value, has been classified to great precision. It's size spans the full length of the full inspiration region and it can be noted that either side of class 4 are the beginnings of non-zero gradients. The other classifications are also in good positions so the overall classification of the respiratory motion is accurate.

In Appendix 1, the classifications for a full 4D volume are shown. These figures show the robustness of the classification as only one respiratory cycle was unable to be classified, Figure 30 and another cycle where the respiratory motion was not a usual cycle, Figure 31.

5.2 Classification of Cardiac Cycles

As seen in Figure 17, the Fast Fourier Transform was a logical step on creating a method to detect the cardiac motion. Due to it's highly oscillatory nature and clearly defined turning points, the Fast Fourier Transform could calculate the period robustly. Since the interval between the turning points, shown in red in Figure 17, are almost constant using the calculated period works well with the "leap frogging" method to clearly determine each of the cycles.

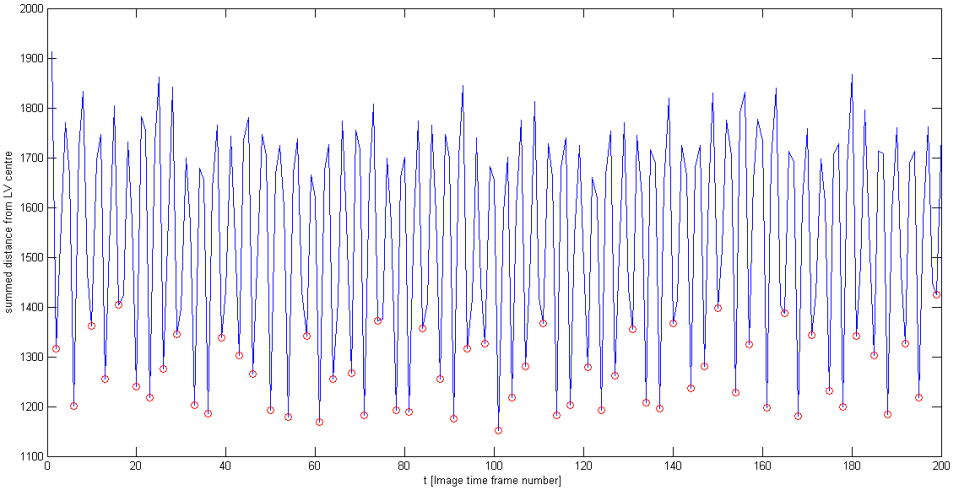

Figure 17: Example of Cardiac cycles with the beginning and end of each cycle identified.

To be certain the classifications were in fact correct, a random selection of frames were viewed manually and checked to see if they correspond to their classification. All appeared to be correct.

5.3 Interpolation of Cardiac Cycles

With the data sorted by their respective classification, both respiratory and cardiac, the final volumes were interpolated. Below in Figures 18, 19 and 20, it shows the interpolated volumes for the respiratory class 5 for each of the three methods used in development.

Figure 18 demonstrates using a smoothing spline to interpolate the volume. Although the initial results look fine, much of the detail in the images are lost. This is due to many frames occupying the same classification, when this occurs the frames are averaged. The most severe case of this is around the $RR = 0.5$, at this time the heart has contracted the most so there is the most movement in the images. As a result, two or more frames have different sizes of myocardium, which causes are blurring effect at the edges.

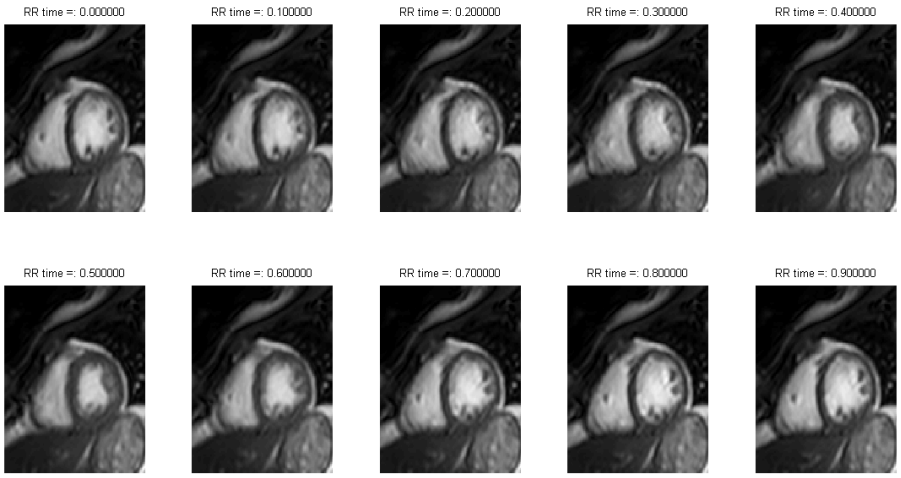

Figure 18: Smoothing Spline interpolation Class 5.

Figure 19 shows a smooth spline with the frame selection method. By selecting the frames, there has been an improvement on observing the motion of the myocardium. As it is seen on frame $RR = 0.5$ the myocardium is more defined in comparison to Figure 18. Further to this the whole set of data is more regular in shape and position due to the frame selection. Although the results have improved, there are still smoothing issues, the contrast between the ventricles and the heart walls are still not strong.

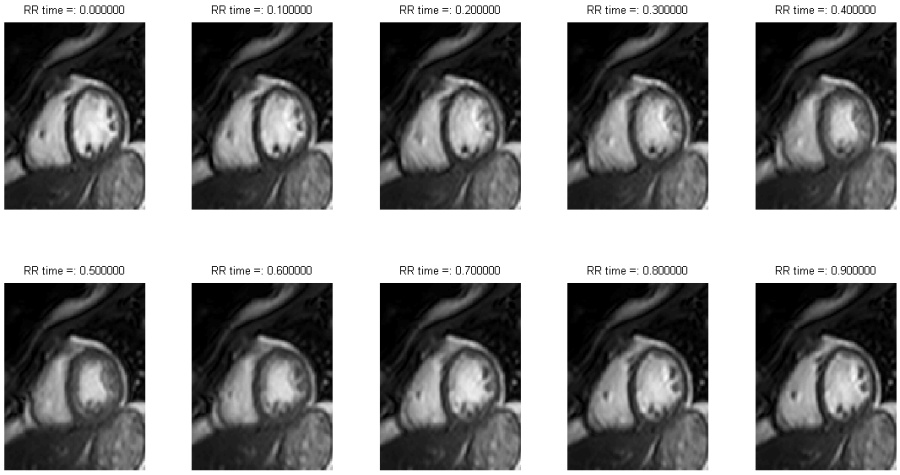

Figure 19: Frame selected, Smoothing Spline interpolation Class 5.

In Figure 20, the best result was achieved. By using the frame selection and the monotonic piecewise cubic spline, a much great definition in the images were gained. The contrasting is the most similar to that of the raw data and the details of the papillary muscles e.t.c. came through well.

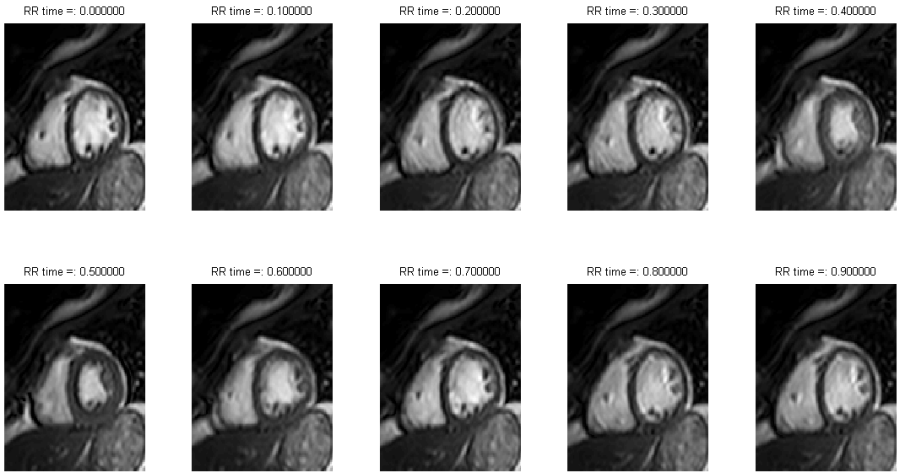

Figure 20: Frame selected, Monotonic Piecewise Cubic Spline interpolation Class 5.

The result of the results can be found in the appendices. Appendix 2 shows the results for all seven respiratory classes for the smoothing spline method. Appendix 3 shows the results for all seven respiratory classes for the frame selection with smoothing spline method. Appendix 4 shows the results for all seven respiratory classes for the frame selection with monotonic piecewise cubic spline method.

As the latter method of interpolation proved to be the best, two RR times were selected to compare the same point of cardiac cycle to determine differences between respiratory classifi-

cations. Below are two figure, Figure 21 is at end-systole (full contraction) and Figure 22 us at end-diastole (full expansion), which are at locations $RR = 0.5$ and $RR = 0$ respectively. It is seen in both figures that the position of the heart moves between frames which is expected since this is the respiratory motion. From these results, it is still difficult to determine heart deformations due to the respiratory motion but a change of shape in the right ventricle can be seen. Deformations in the left ventricle cannot be seen in Figure 21 because the respiratory motion forces are negligible in comparison to the hearts contraction. In Figure 22, deformations of the left ventricle can be seen. In classifications 1 and 7 the left ventricle has a more circular shape where as in class 4, the left ventricle has deformed to flatter bottom. This result would seem reasonable since at class 4 (full inspiration) is when the diaphragm is pushing most against the heart causing this flat bottom effect.

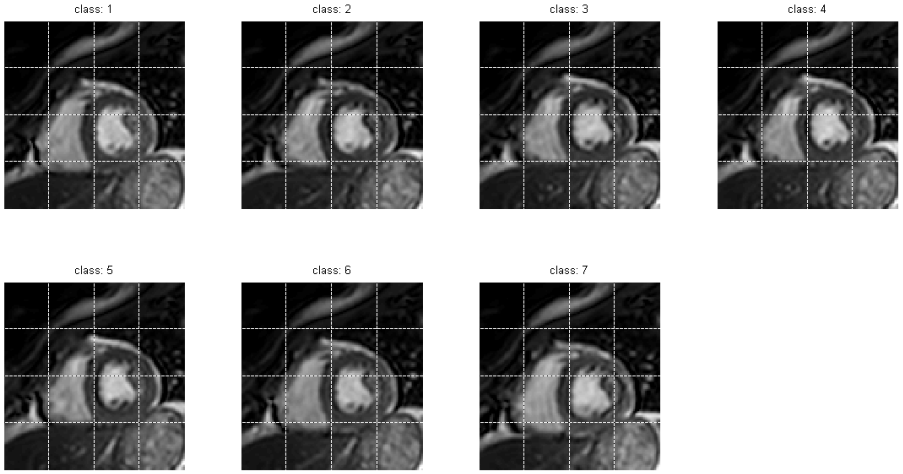

Figure 21: Example of systole for each of the respiratory classes

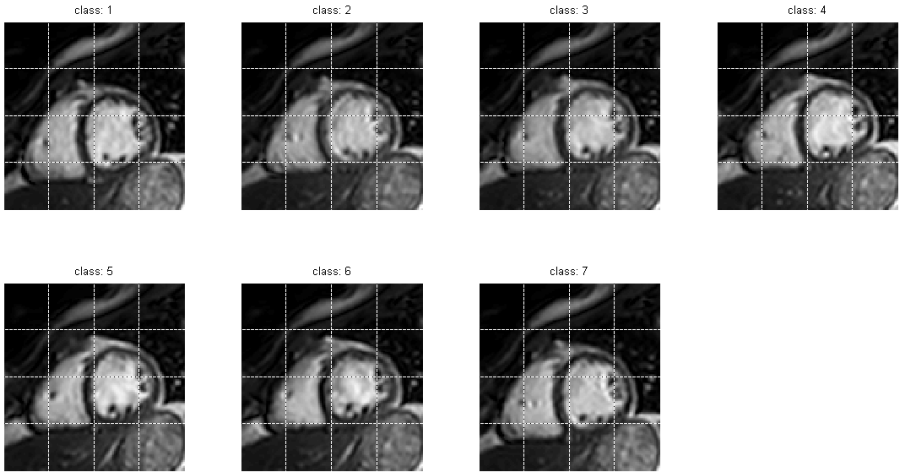

Figure 22: Example of diastole for each of the respiratory classes

5.4 Analysis of Interpolated Cardiac Cycles to Determine Differences in Volume for the Left Ventricle

To determine the clarity of the interpolation methods and to compare these results with known physiological facts, the ejection fraction was calculated. The ejection fraction (EF) quantifies the volume of blood pumped out of the left ventricle for each of the cardiac cycles. The interpolated volumes had there left ventricles delineated to determine the change of volumes. The ejection fraction compares the volume of the end-diastolic volume (EDV) with the end-systolic volume (ESV) using the equation:

$$EF[\%] = \frac{EDV[ml] - ESV[ml]}{EDV[ml]} \tag{15}$$

The normal range of a ejection fraction is $55 - 70\%$ [14]. For comparison of methods the same slice was used to calculate the ejection fraction and only one slice so the values are relative to this slice and not a true representation of the left ventricle volume as seen in table below, Table 1, and in Figure 23 which is the ejection fraction represented in graphical form to easily compare the methods.

Method	1:Smoothing Spline			2:Frame selection, Smoothing Spline			3:Frame selection, Cubic Spline		
Class	EDV [ml]	ESV [ml]	EF [%]	EDV [ml]	ESV [ml]	EF [%]	EDV [ml]	ESV [ml]	EF [%]
1	19	14	26.3158	19	15	21.0526	18	10	44.4444
2	18	15	16.6667	17	12	29.4118	18	11	38.8889
3	17	15	11.7647	18	14	22.2222	17	10	41.1765
4	17	15	11.7647	17	12	29.4118	17	10	41.1765
5	18	16	11.1111	16	13	18.7500	17	10	41.1765
6	17	16	5.8824	15	9	40.0000	16	8	50.0000
7	20	15	25.0000	18	13	27.7778	17	11	35.2941
mean	18.0000	15.1429	15.5008	17.1429	12.5714	26.9466	17.1429	10.0000	41.7367
St. dev. ±	1.1547	0.6901	7.6186	1.3452	1.9024	7.1587	0.6901	1.0000	4.5857

Table 1: Ejection Fraction of interpolation methods

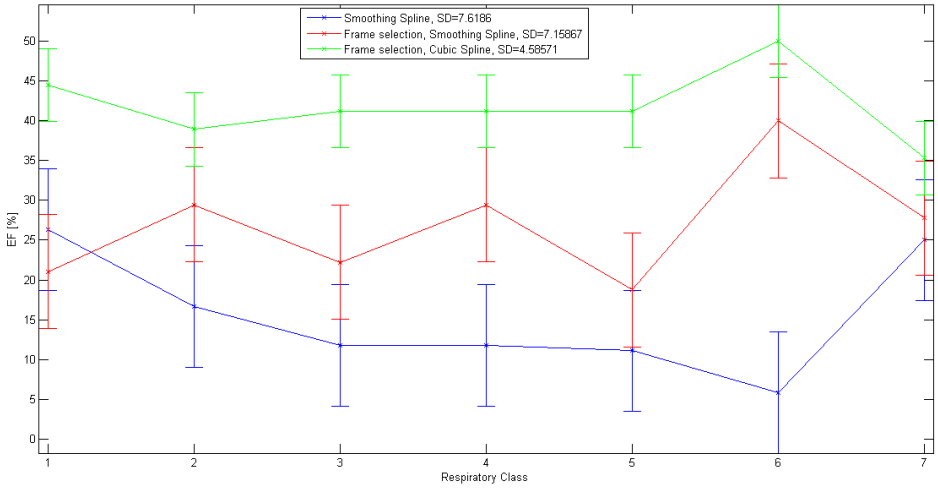

Figure 23: Ejection Fraction for each of the respiratory classes and interpolation methods

From looking at Figure 23, it is noted that the mean ejection fraction increases with the improvements in the interpolation methods. This is a good result as it shows that the improvements to the interpolation methods more accurately represents known information. Since the

latest method is nearing the normal range with a smaller standard deviation, it implies that the result is also more consistent for all respiratory cycles. The mean ejection fraction for the best method is still out with the normal range but this may be due to only using one slice instead of the whole volume.

Using the best method, a 4D volume was created for each of the respiratory cycles. From this data the full volume ejection fraction was calculated to see if it conforms with the medical data, Table 2 and Figures 24, 25, 26 shows the results. To calculate errors, since only one set of volumes have been create so far due to limited MRI data, a reading error of $\pm 0.5\ ml$ was given to each of the slices volumes. By combining errors the total volumes have an error of $\pm\sqrt{1.25}\ ml$ and the ejection fraction error is calculated by;

$$EF\ error = \pm EF \times \sqrt{\left(\frac{\sqrt{1.25}}{ED - ES}\right)^2 + \left(\frac{\sqrt{1.25}}{ED}\right)^2} \tag{16}$$

Class	1		2		3		4		5		6		7	
Slice (top - bottom)	EDV [ml]	ESV [ml]	EDV [ml]	ESV [ml]	EDV [ml]	ESV [ml]	EDV [ml]	ESV [ml]	EDV [ml]	ESV [ml]	EDV [ml]	ESV [ml]	EDV [ml]	ESV [ml]
6000	19	9	20	10	20	9	18	9	18	9	19	8	19	8
45000	18	8	17	8	17	8	17	8	16	7	16	7	18	9
32000	16	8	17	8	16	7	16	6	15	7	15	11	16	7
28000	14	6	15	6	13	6	14	5	13	6	15	6	14	7
7000	12	6	11	4	11	5	9	4	10	5	9	4	12	4
sum	79	37	80	36	77	35	74	32	72	34	74	36	79	35
EF [%]	53.1646		55		54.5455		56.7568		52.7778		51.3514		55.6962	
EF error [± %]	1.6028		1.5950		1.6539		1.7372		1.7558		1.6984		1.6199	

Table 2: Full 4D volume Ejection Fraction

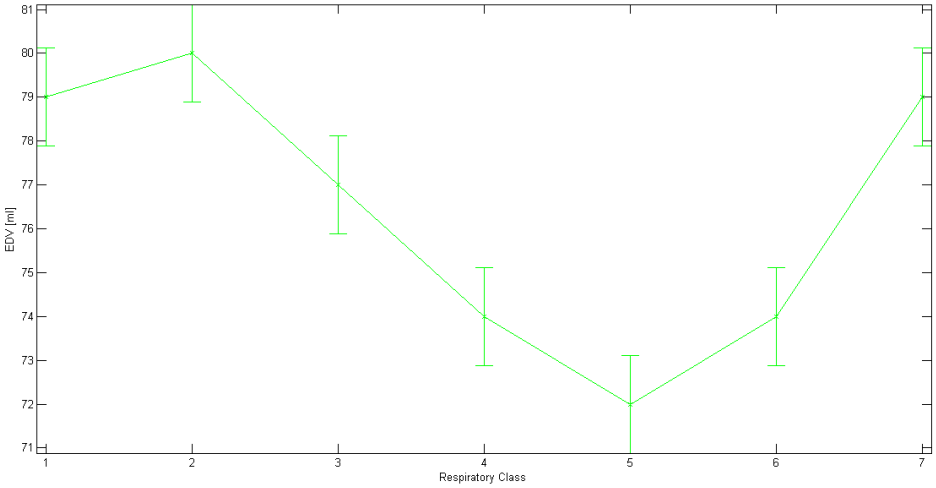

Figure 24: End-Diastole Volume for each of the respiratory classes for full 4D volumes

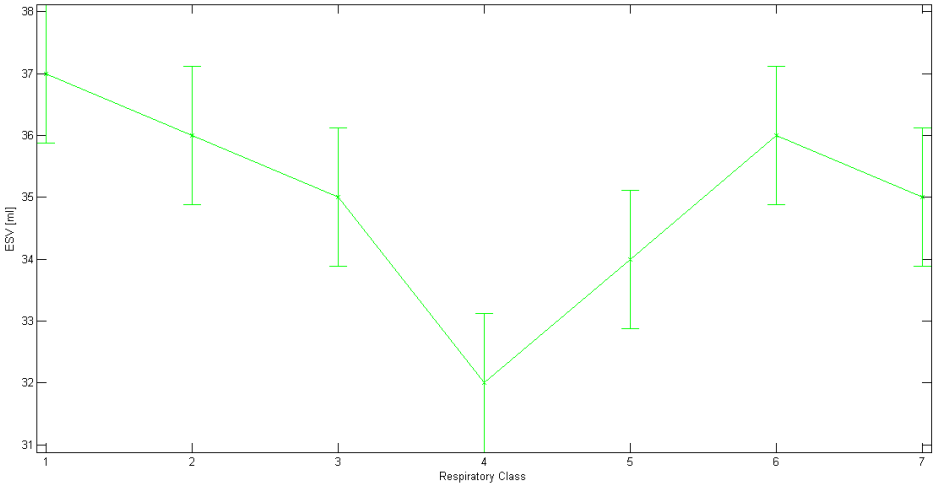

Figure 25: End-systole Volume for each of the respiratory classes for full 4D volumes

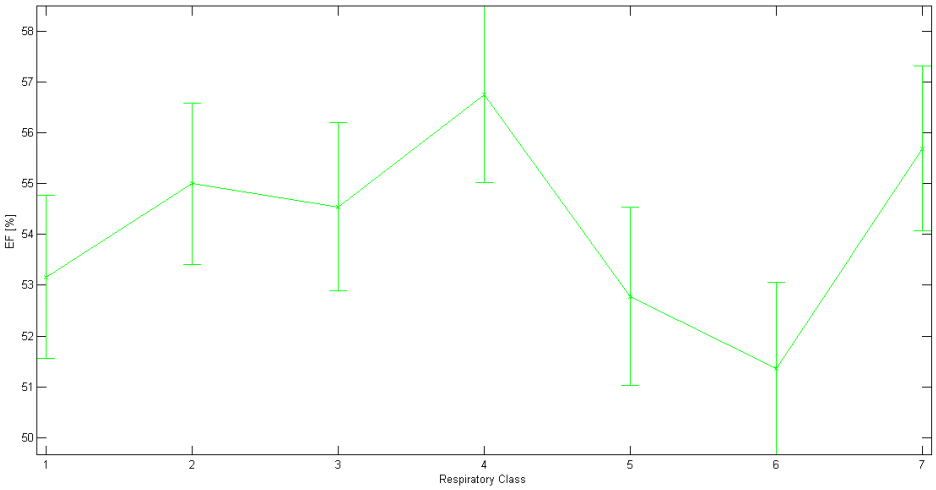

Figure 26: Ejection Fraction for each of the respiratory classes for full 4D volumes

As it is seen in Figure 26, some of the points and most of the error ranges are within the medical normal of $55 - 70\%$. This is a promising result, as it shows that these simulations do have a feasible cardiac motion comparable to that of previous ways of acquiring cardiac MR images. The current standard is to look at the ejection fraction when the patient has full expiration, from the results, this is the value at class 7 which is $55.6962 \pm 1.6199\%$.

Further to this, by looking at Figures 24, 25, it can be noted that these results have a correlation to the respiratory motion. At the point when class 4 changes to class 5, this is the point of when inspiration is at its fullest. As mentioned before, the left ventricle seems to deform into flat bottomed circle when the diaphragm has expanded which implies that the left ventricle will lose volume. The result gives an initial confirmation to that idea, as they have a parabolic shape and the local minima points in Figures 24, 25, are at class 4 and class 5.

6 Discussion and Conclusions

Overall this thesis has been a success. The method created, uses real-time cine cardiac magnetic resonance imaging to accurately represent cardiac motion at multiple respiratory phases. The classification method robustly categorises each of the images then the interpolation method uses this accordingly. The information presented from this method gives a deeper insight to the forces on the heart and gives a tool to be used by physiologists. From the initial results it can be seen that the heart does change in volume during respiratory motion which with further research opens a discussion for physiologist on which respiratory phases gives the most useful information. In addition this, by creating this method, it has the potential of being an option for patients in the future, to obtain cardiac MRI data in a faster and less distressing way as the patient would not be required to hold their breath, which is also difficult for some patients.

The main pitfall of this method would be the range of data that this method would work for. A known issue would be that the cardiac magnetic resonance image has to be in an orientation where the left and right ventricles are side by side, with the right ventricle on the left hand side of the image. Another problem is that the data must contain enough respiratory cycles. If not, then there is not enough data to appropriately fill the classification bins. When there is a sparse set of data, the interpolation method has difficulties to interpolate accurately. The temporal resolution must also be of a high enough resolution so the cardiac cycles can be observed. The current data would be the minimum temporal resolution of 218.4 ms as this is around 4 frames per cardiac cycle, anything less than this, the cardiac cycle cannot be observed.

If I were to have more time on this thesis, I would have liked to have tried to improve the interpolation method. Currently the method does not observe adjacent voxels. By doing so, more accurate interpolations can be made which could lead to improving the spacial resolution. One method that I would propose would be to use Optical Flow. Optical Flow creates a directional mapping for pixels of similar intensity between adjacent time frames. Further to this, since the left ventricle perimeters are known then this can be used to influence the direction of the mapping.

Another way to improve the image quality would be instead of selecting frame to interpolate from, using the selection method to create a reference frame for all other frames occupying the same classification to be warped and then averaged. By doing so the signal to noise ratio of the interpolated data would be greater and then it can be used to increase the spacial resolution again.

Other areas for improvement would be the computational time. Currently one slice would take around 10 minutes to compute interpolated volumes on a 2.5 GHz quad core processor. All instances for parallelization within the method have already been pursued but at points in the method, such as calculating the surface for the respiratory motion, is highly expensive in memory use and computation time. For these instances a compromise in accuracy for a faster method may be more suitable in the hope that the robustness of the classification method could compensate.

References

[1] Martin A. Fischler and Robert C. Bolles *Random Sample Consensus: A Paradigm for Model Fitting with Applications to Image Analysis and Automated Cartography* Comm. of the ACM 1981 Jun; 24 (6): 381395. doi:10.1145/358669.35869

[2] J. B. MacQueen, *Some Methods for classification and Analysis of Multivariate Observations* In Proceedings of Proceedings of 5th Berkeley Symposium on Mathematical Statistics and Probability(1), pp. 281-297, Berkley, 1967

[3] World Health Organisation, `http://www.who.int/mediacentre/factsheets/fs310/en/`, July 2013.

[4] Peter Kellman, Christophe Chefdhotel, Christine H. Lorenz, Christine Mancini, Andrew E. Arai, Elliot R. McVeig, *Fully automatic, retrospective enhancement of real-time acquired cardiac cine MR images using image-based navigators and respiratory motion-corrected averaging.*,John Wiley & Sons, Inc., Magn Reson Med. 2008 Apr;59(4):771-8. doi: 10.1002/mrm.21509.

[5] Heiberg, Einar and Sjögren, Jane and Ugander, Martin and Carlsson, Marcus and Engblom, Henrik and Arheden, Håkan, *Design and validation of Segment - freely available software for cardiovascular image analysis*, BMC Medical Imaging, Vol. 10, (2010).

[6] ZooFari, Wikipedia `http://en.wikipedia.org/wiki/File:Heart_diagram-en.svg`, March 2010.

[7] Michael Kirby, *Geometric Data Analysis: An Emperical Approach to Dimensionality Reduction and the Study of Patterns*, John Wiley & Sons, Inc., Publication (2001).

[8] J. T. Tou, R. C. Gonzalez, *Pattern Recognition Principles*, Addison-Wesley Publishing Company (1974).

[9] B. D. Ripley, *Pattern Recognition And Neural Networks*, Cambridge University Press (1996).

[10] Geof H. Givens, Jennifer A. Hoeting, *Computational Statistics*, John Wiley & Sons, Inc., Publication (2005).

[11] J. P. Marques de Sá, *Pattern Recognition: Concepts, Methods and Applications*, Springer-Verlag Berlin Heidelberg New York (2001).

[12] D. Kahaner, C. Moler, and S. Nash, *Numerical Methods and Software*, Prentice Hall, Englewood Cliffs, NJ, (1989).

[13] F. N. Fritsch, R. E. Carlson. *Monotone Piecewise Cubic Interpolation* SIAM Journal on Numerical Analysis (SIAM) 17(2):238246. doi:10.1137/0717021 (1980).

[14] Simon O'Connor, *Examination Medicine (The Examination)*. Edinburgh: Churchill Livingstone. p.41. ISBN:0-7295-3911-3. (2009)

[15] Petter Dyverfeldt *Extending MRI to the Quantification of Turbulence Intensity* Linköping Studies in Science and Technology Dissertation, No. 1297 (2010).

7 Appendices

7.1 Appendix 1: Classification of Respiratory Cycles for Full 4D Volumes

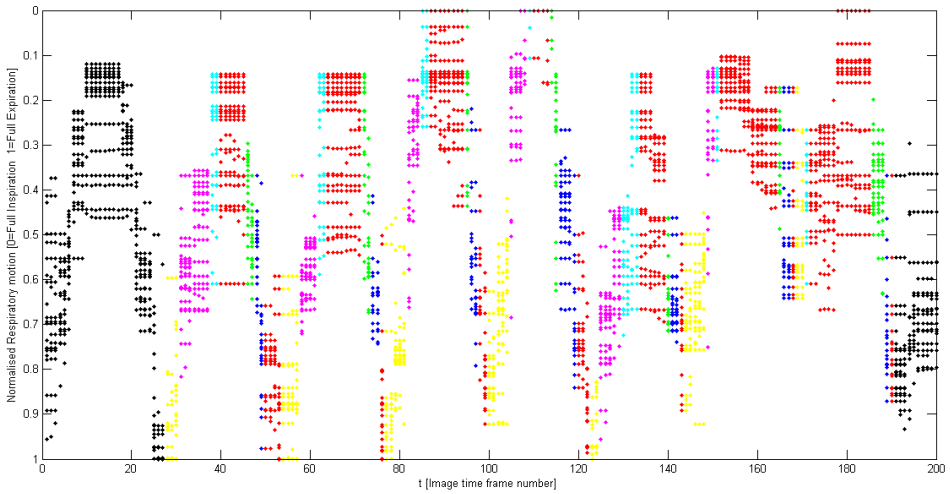

Figure 27: Classification of Respiratory cycle for slice 6000.

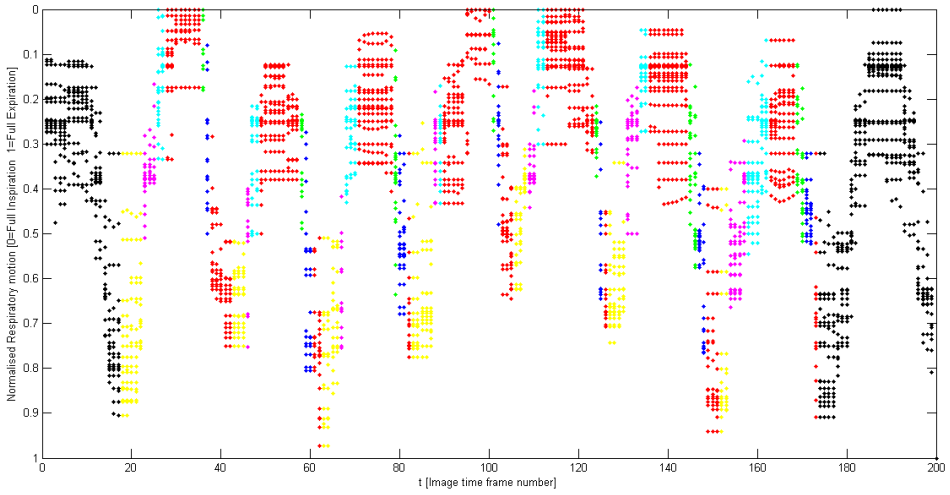

Figure 28: Classification of Respiratory cycle for slice 45000.

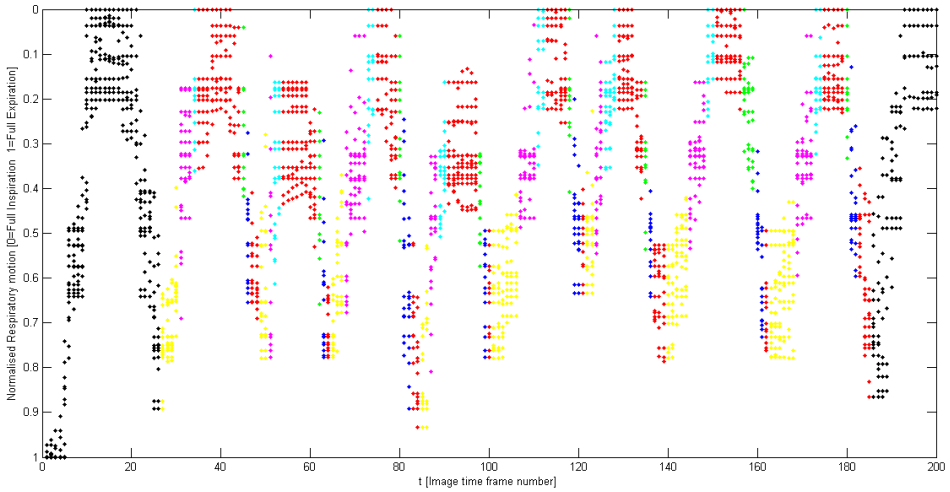

Figure 29: Classification of Respiratory cycle for slice 32000.

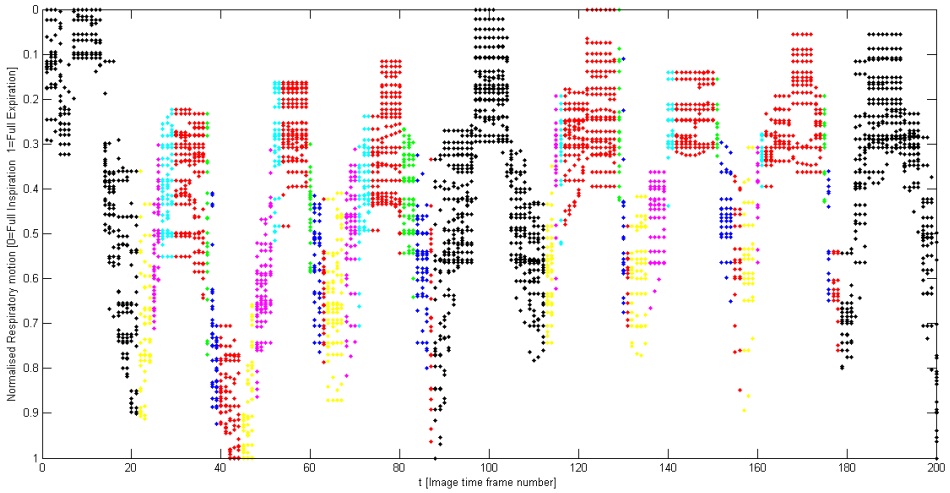

Figure 30: Classification of Respiratory cycle for slice 28000.

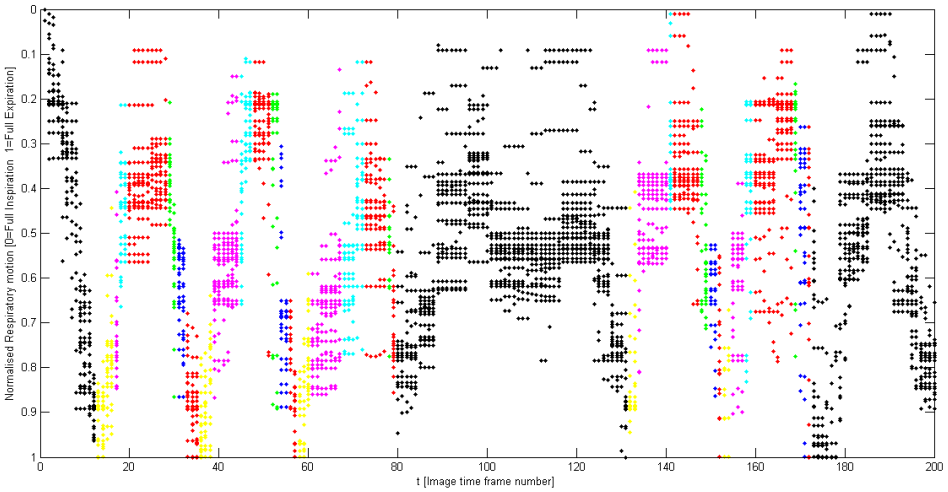

Figure 31: Classification of Respiratory cycle for slice 7000.

7.2 Appendix 2: Smoothing Spline Method Results

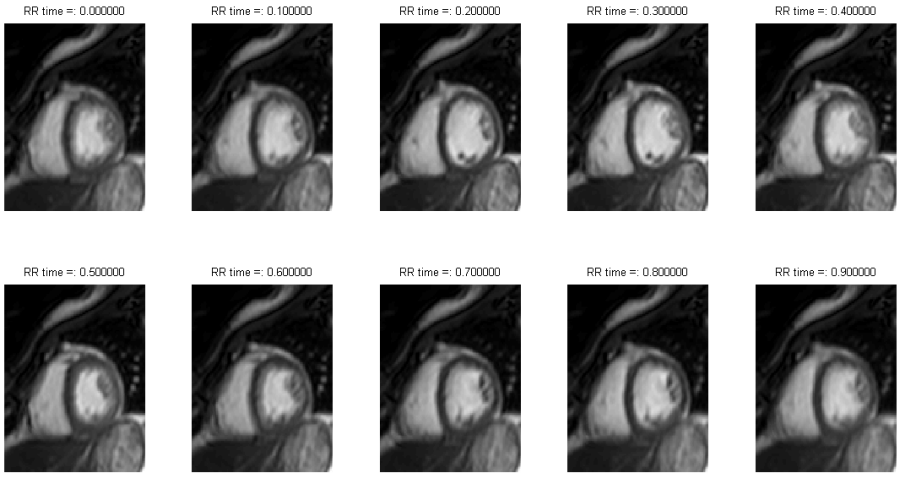

Figure 32: Smoothing Spline interpolation Class 1.

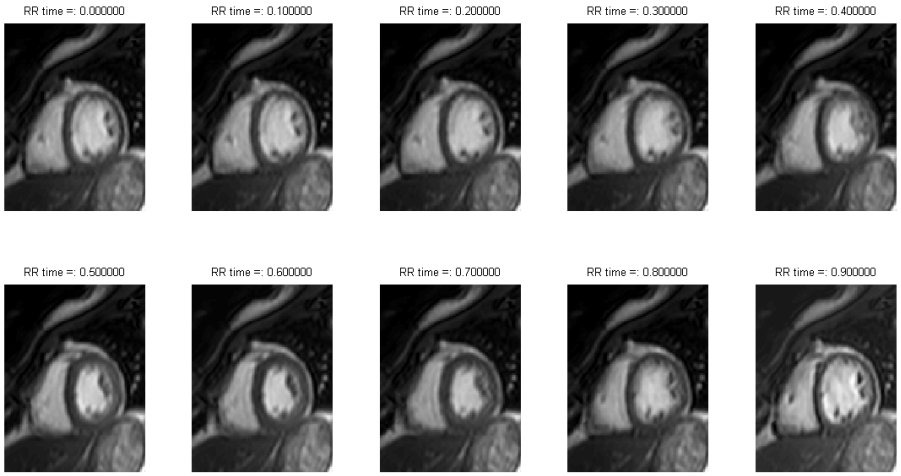

Figure 33: Smoothing Spline interpolation Class 2.

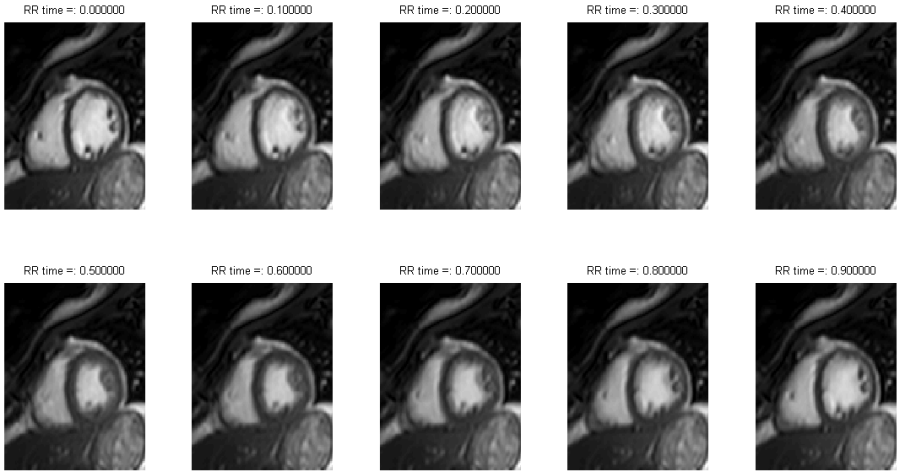

Figure 34: Smoothing Spline interpolation Class 3.

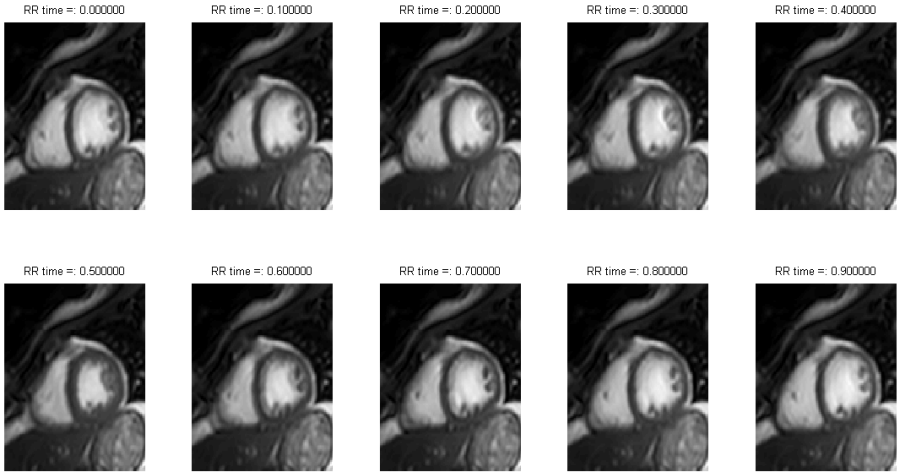

Figure 35: Smoothing Spline interpolation Class 4.

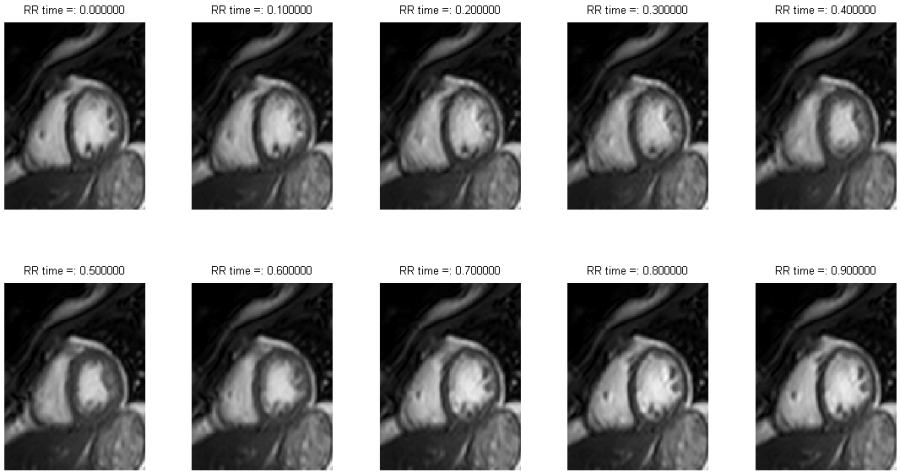

Figure 36: Smoothing Spline interpolation Class 5.

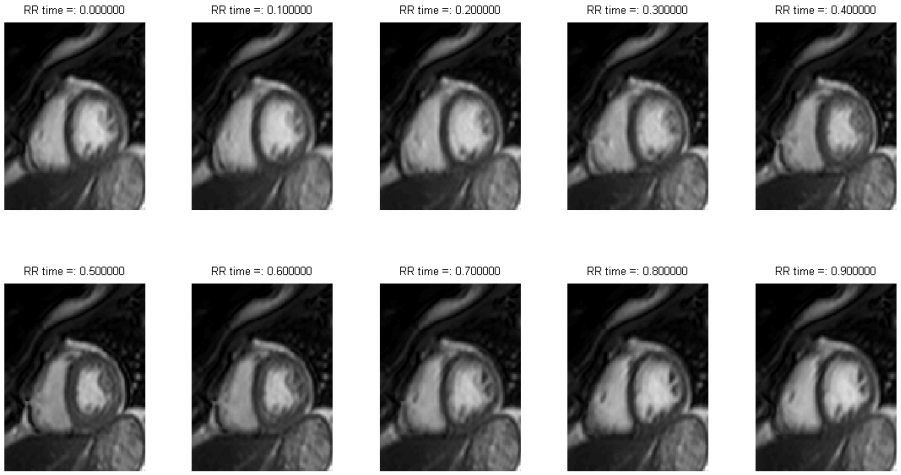

Figure 37: Smoothing Spline interpolation Class 6.

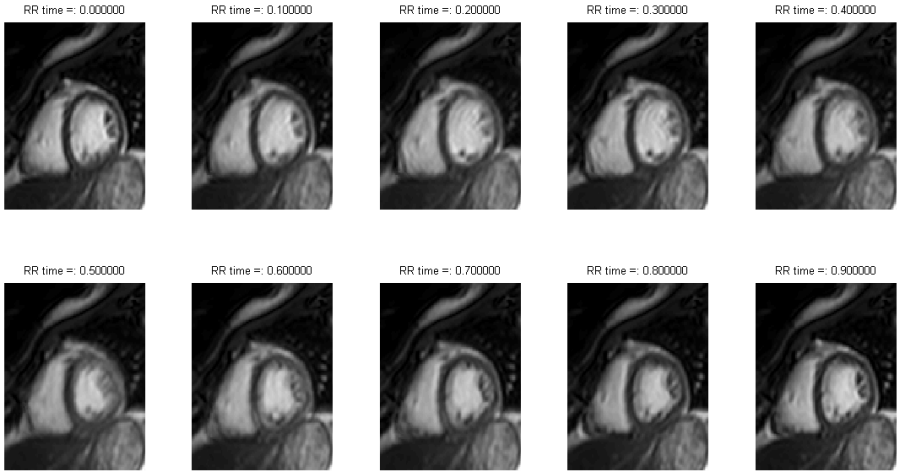

Figure 38: Smoothing Spline interpolation Class 7.

7.3 Appendix 3: Frame Selection with Smoothing Spline Method Results

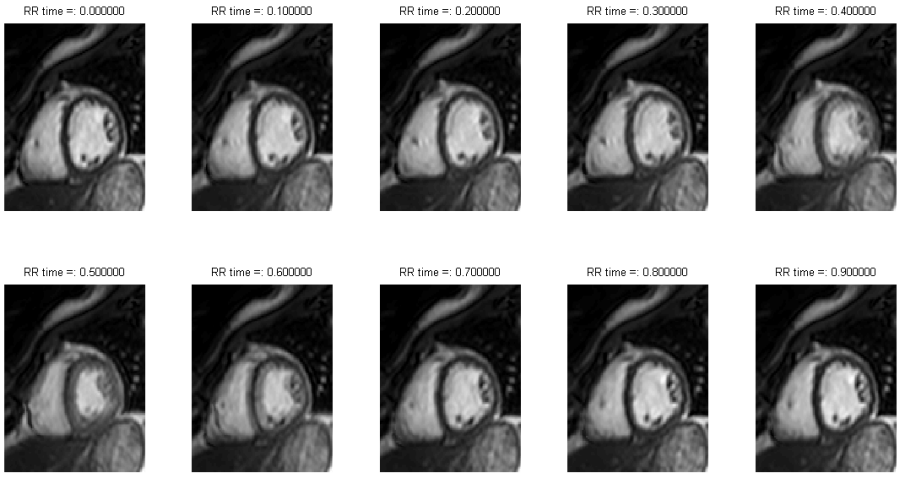

Figure 39: Frame selected, Smoothing Spline interpolation Class 1.

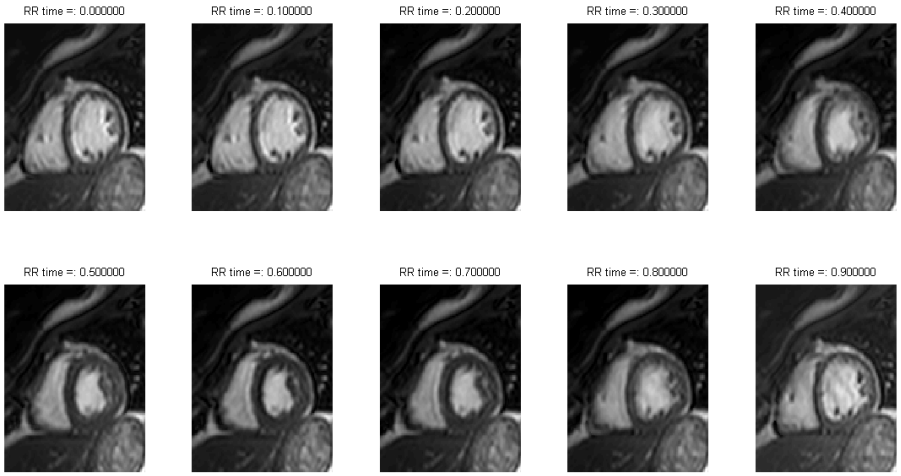

Figure 40: Frame selected, Smoothing Spline interpolation Class 2.

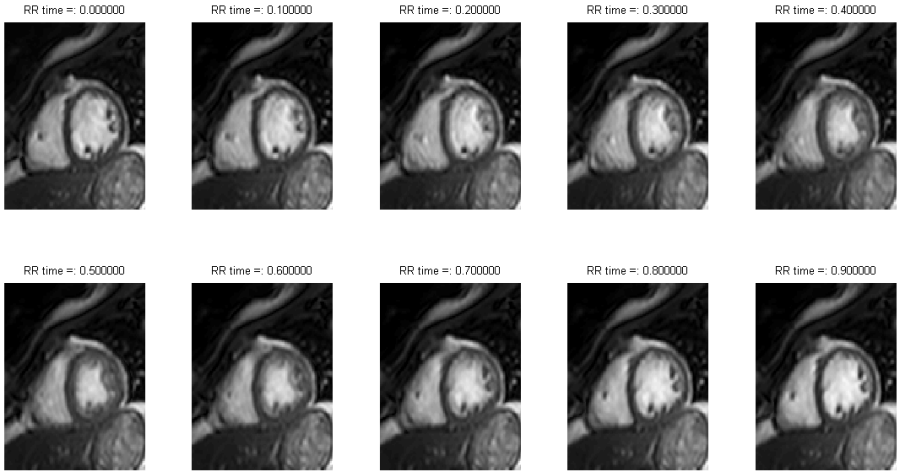

Figure 41: Frame selected, Smoothing Spline interpolation Class 3.

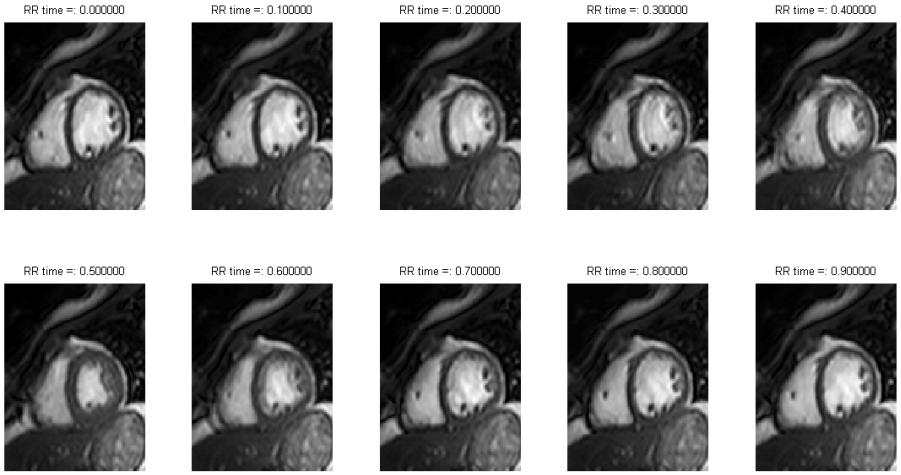

Figure 42: Frame selected, Smoothing Spline interpolation Class 4.

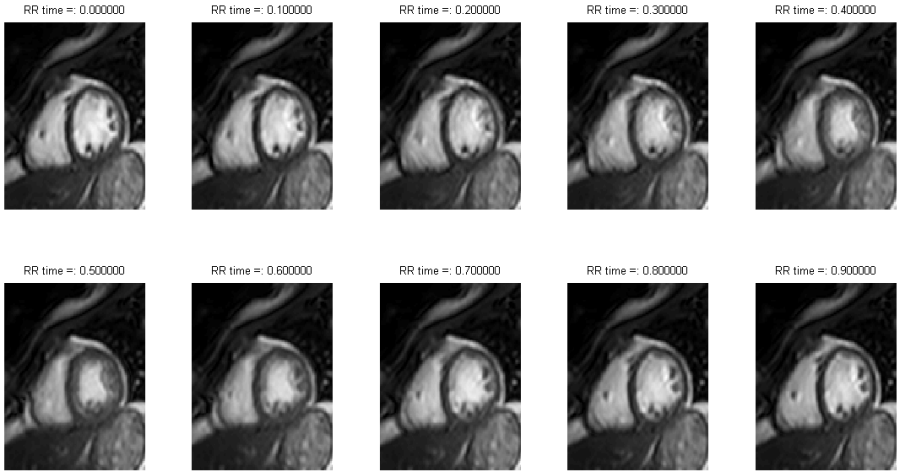

Figure 43: Frame selected, Smoothing Spline interpolation Class 5.

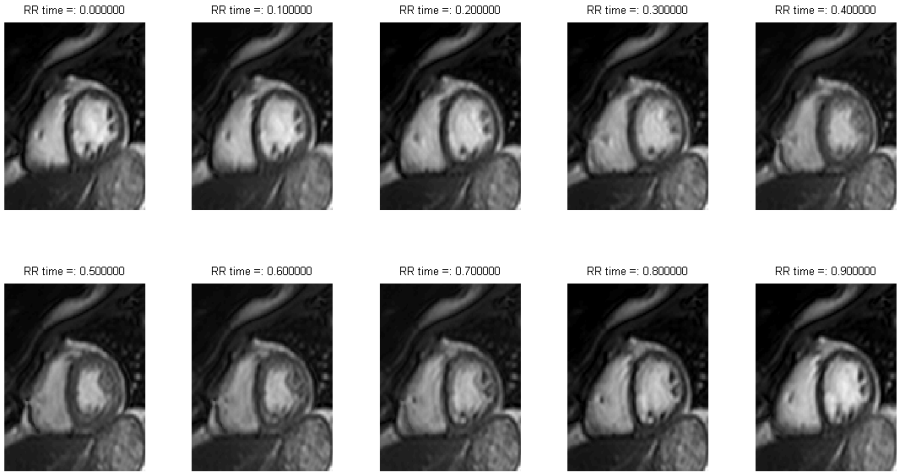

Figure 44: Frame selected, Smoothing Spline interpolation Class 6.

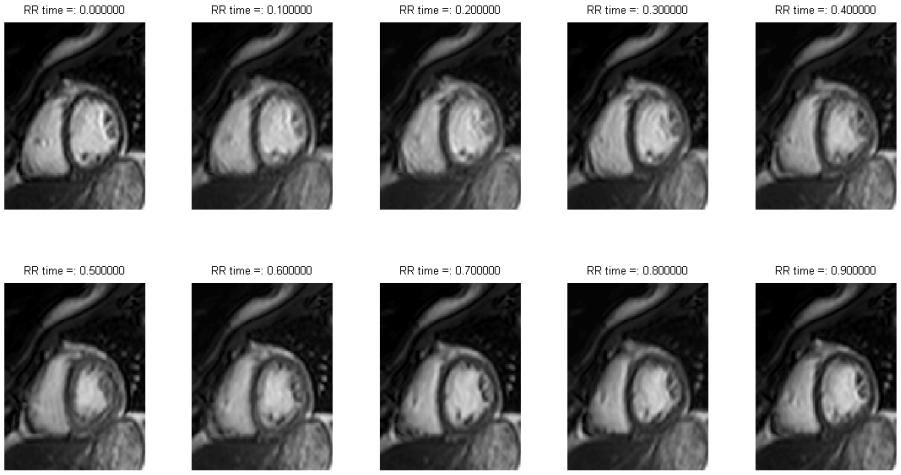

Figure 45: Frame selected, Smoothing Spline interpolation Class 7.

7.4 Appendix 4: Frame Selection with Monotonic Piecewise Cubic Spline Interpolation Method Results

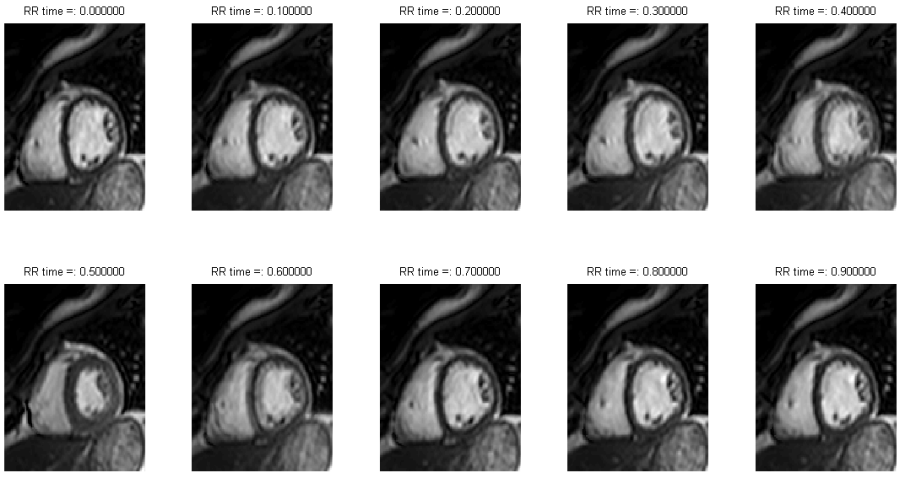

Figure 46: Frame selected, Monotonic Piecewise Cubic Spline interpolation Class 1.

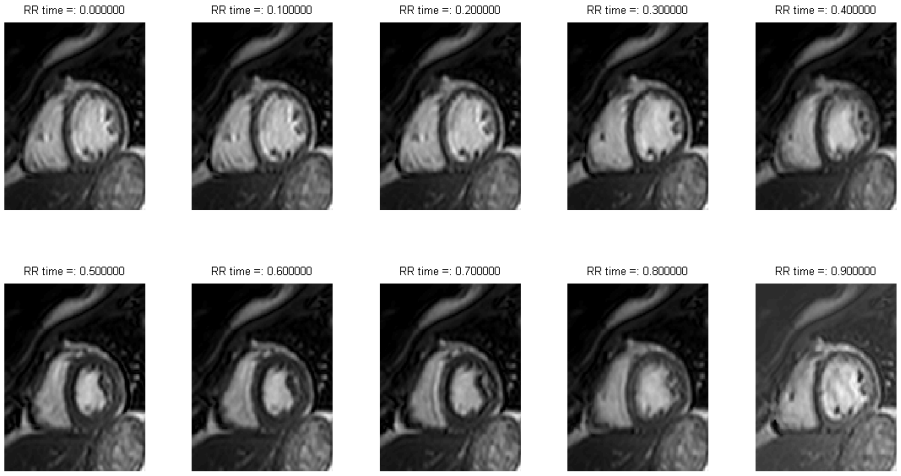

Figure 47: Frame selected, Monotonic Piecewise Cubic Spline interpolation Class 2.

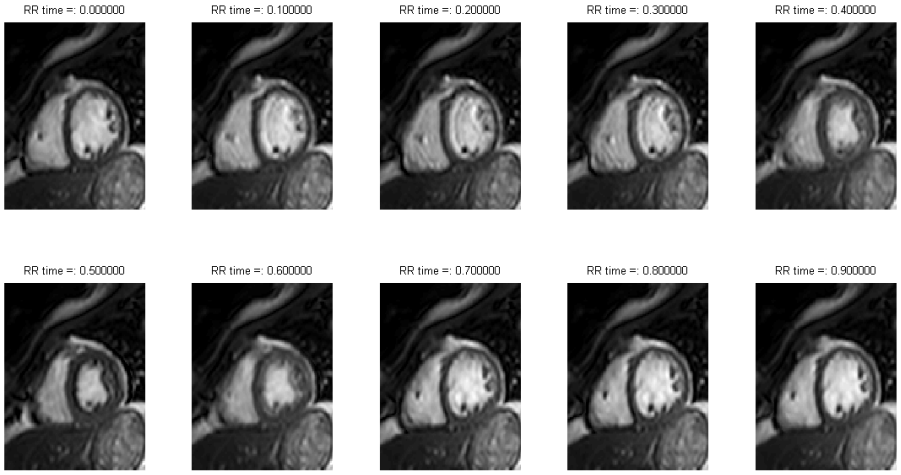

Figure 48: Frame selected, Monotonic Piecewise Cubic Spline interpolation Class 3.

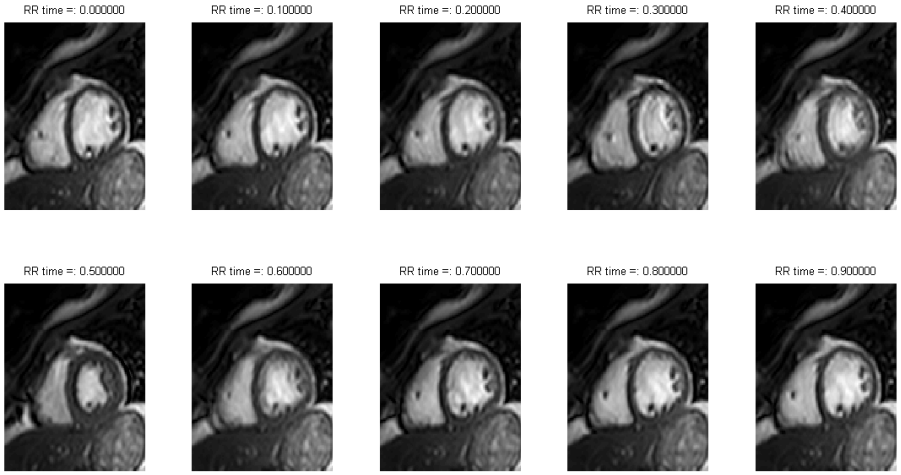

Figure 49: Frame selected, Monotonic Piecewise Cubic Spline interpolation Class 4.

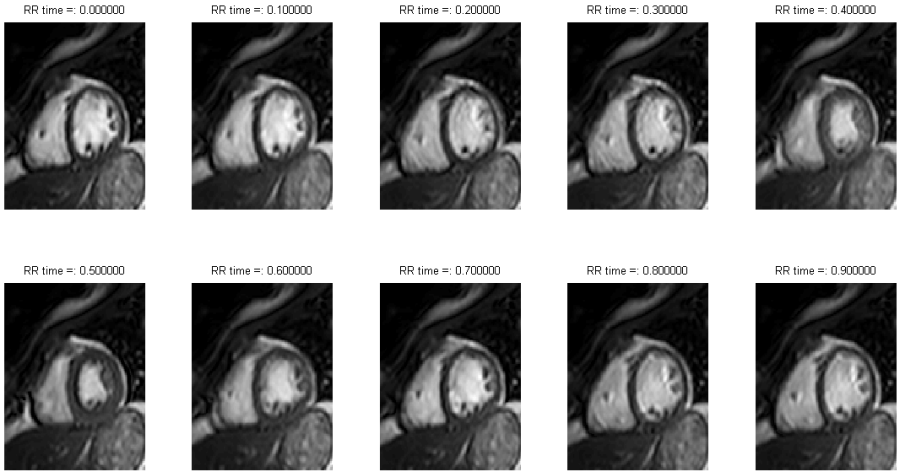

Figure 50: Frame selected, Monotonic Piecewise Cubic Spline interpolation Class 5.

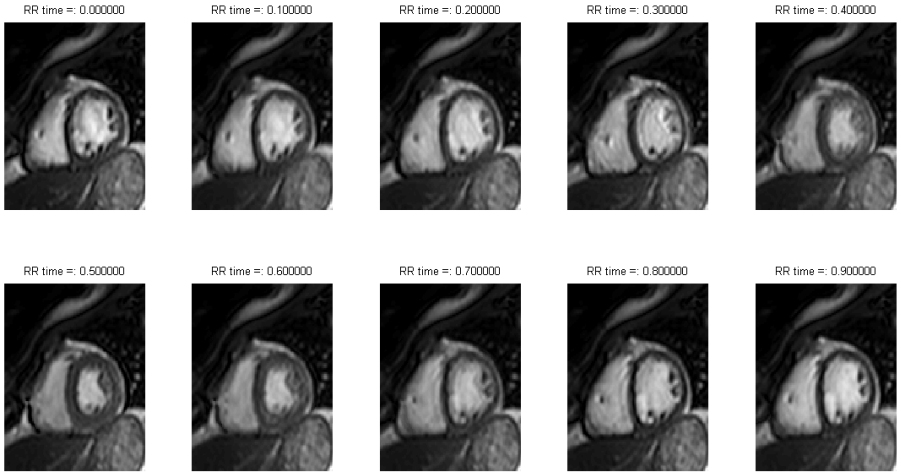

Figure 51: Frame selected, Monotonic Piecewise Cubic Spline interpolation Class 6.

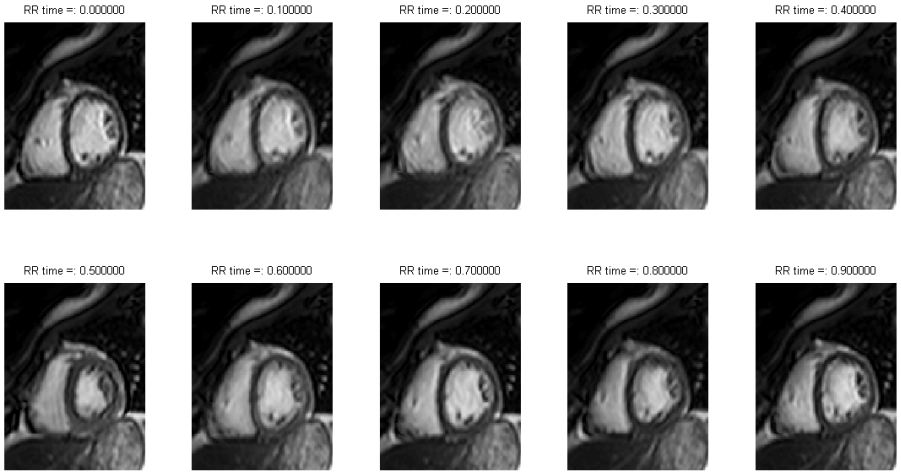

Figure 52: Frame selected, Monotonic Piecewise Cubic Spline interpolation Class 7.

Master's Theses in Mathematical Sciences 2014:E28
ISSN 1404-6342

LUNFNA-3017-2014

Numerical Analysis
Centre for Mathematical Sciences
Lund University
Box 118, SE-221 00 Lund, Sweden

http://www.maths.lth.se/